AUT Journal of Modeling and Simulation

AUT J. Model. Simul., 53(2) (2021) 113-136
DOI: 10.22060/miscj.2021.19648.5241

Hardware-in-the-Loop Motion Simulator of Quadrotor: Analysis of Autonomous Trajectory Tracking

H. Khajvand, M. R. Homaeinezhad*

Faculty of Mechanical Engineering, K. N. Toosi University of Technology, Tehran, Iran

ABSTRACT: Direct trajectory tracking of quadrotor system in 3D space is not possible originating from the fact that control inputs are not independent in manipulating all flying degrees of freedom. The major concentration of the presented study is to describe the design procedure of a new intelligent algorithm for moving the quadrotor along a trajectory curve in space. The presented algorithm consists of two major parts. In the primary one, the desired Euler angles and their associated rates are intelligently estimated by a Fuzzy Logic Controller (FLC) working based on the experimentally Fuzzyfied rules. The second part of the proposed algorithm is the Sliding Mode Control (SMC) designed for precise tracking of the commanded Euler angles while guaranteeing the robust stability of the quadrotor flight. To simulate the airborne performance of the quadrotor equipped with the proposed trajectory algorithm, a heavy-duty 6-DOF Hardware-In-the-Loop Motion Simulator (HILMS) by which all motions of a quadrotor (either translational or rotational movements) can be precisely evaluated, is designed and fabricated. The introduced HILMS employs one load cells for each arm of the quadrotor, allowing the microcontroller to access to the thrust of the motors during operation. This way, while the translational motion is restricted, the position of the quadrotor can be computed along the governing mathematical motion equations. The empirical results confirm stability and trajectory tracking quality of the quadrotor by implementation of the proposed two-staged intelligent algorithm.

Review History:

Received: Feb. 16, 2021
Revised: Dec. 09, 2021
Accepted: Dec. 25, 2021
Available Online: Mar, 10, 2022

Keywords:

Motion Simulator
Hardware-In-the-Loop
Fuzzy Logic Control
Sliding Mode Control
Path Following; Trajectory Tracking

1- Introduction

Quadrotor, a well-known flying vehicle with fairly simple governing equations of motion, has been an interesting subject for many researchers for the last few years. Although, a quadrotor can be controlled by an expert pilot through a radio control, the autonomous position control of a quadrotor using conventional sensor systems such as GPS, INS, and ultrasonic sensors is however on its preliminary stages.

Due to atmospheric disturbances, power limitations, under-actuated nature of the quadrotor, plant uncertainties, and navigation sensor's drift in the outdoor applications, autonomous guidance of a quadrotor is a complicated fatal work. Its repetition requires high financial support alongside its probable risks and crashes for a long time in order to elaborate a robust and disturbance-tolerant control algorithm. In order to find an acceptable solution for autonomous flight of a quadrotor, a test-bed is required to simulate the translational motion of the system where so many repetitions become possible. Additionally, appropriate hardware, which is capable of performing designed algorithms while not being very different from conventional microcontrollers embedded on the commercially applied quadrotors, must be used.

Despite the suitable performance and robustness of the fuzzy-based controllers, their application to the quadrotor is almost limited to simulation studies due to three reasons. First, the computational burden of the fuzzy controllers is heavy, meaning that their application in an ordinary embedded processor, the number of rules, fuzzification/defuzzification algorithms and inference techniques should be designed optimally by scrupulously arranged experiments. Second, a lack of simulator for trying numerous tests in order to find a final solution prevents the designer to bring the algorithms from simulation stages to real applications. Third, when the stability proof of the fuzzy controllers is a hard task when being designed, which causes their limited real applications relative to conventional PID or sliding mode controllers.

As a review to the previous works, in order to verify new controllers in the study of [1], developing a Hardware-In-the-Loop simulator by using a complete mathematical model of the UAV, including the external variables, is discussed. Additionally, experimental platform is presented to validate the HIL implementation. The study of [2] worked on developing an interface for rapid prototyping of control strategies within Matlab Simulink with the help of a mono-camera tracking system. The accuracy of the system is evaluated theoretically and experimentally for HILS, using Simulink blocks. The results of the development of an indoor quadrotor with the focus on accurate position and orientation sensing are

*Corresponding author's email: mrhomaeinezhad@kntu.ac.ir

presented in [3]. The system was described for both HIL and normal operation. The design, real-time implementation and testing of the control and diagnostic functions of a quadrotor, using a Network Control System is discussed in [4]. A HIL simulator with a real-time simulated model of the drone has been set up, and the results of the real time implementation and the simulation results using Matlab/Simulink and Truetime toolbox are compared. A HIL simulation setup for multi-UAV systems is presented in [5]. Using this system, the algorithms are tested directly on the onboard computational units; Moreover, the communication among multiple boards became available. A flexible test-bed derived control method for quadrotor is described in [6]. The main objective of this HIL system is testing ordinary controllers for quadrotor real-time orientation movements. It is shown that, the performance evaluation, implementation and tuning the required gain constants can be made easily and user-friendly in real-time operations. A direct approximate-adaptive control, which uses Cerebellar Model Arithmetic Computer (CMAC), is applied on an experimental quadrotor test-bed to control the attitude angles [7]. The proposed method updates adaptive parameters in order to adjust the system to unknown payloads and to achieve enough robustness. In the attitude experimental tests, the method prevents the drift of impulse disturbances, where the adaptation mechanism converges to the value of unknown payload masses. In [8], an adaptive sliding mode control method is issued on a quadrotor to investigate uncertainty problems. Simulations demonstrate acceptable results for stability and tracking control. Finally, the design, development, and testing of a stabilizing control algorithm devised for a quadrotor using Mamdani fuzzy logic controller is presented, which the implementation of this controller is based on trial and error method [9]. With the main focus on the maneuverability of this vehicle, the obtained results indicated that the fuzzy based stabilizing control system is more accurate in high dynamic disturbances compared to the traditional systems which used PID integrated stabilizer control algorithms. Comprehensive literature review shows that Linear Quadratic Regulator (LQR) and linear control methods, such as PID controllers, are widely used to enhance the stability of quadrotors [10-13].

Furthermore, related works to the simulators that have the ability to control the translational motion of a quadrotor are discussed as follows. A control algorithm which is based on backstepping approach is implemented on a quadrotor with the help of vision system, inertial measurement unit, and Kalman filter state estimator in [14]. Using a HILS, the path tracking results of the system is shown. The study of [15] introduces a HIL platform which is capable of simulating and testing UAVs with different mathematical models and control strategies. The main focus of this survey is the integration of modeling, control, simulation, experimentation and data display. Another study presents two types of nonlinear controllers for position control of a quadrotor [16]. The first approach is feedback linearization controller which involves high order derivative terms, and the second algorithm is adaptive sliding mode controller using input augmentation. Simulation results show that feedback linearization controller is sensitive to sensor noise and modeling uncertainty, while adaptive sliding mode controller achieves better performance under noisy conditions, which indicates that adaptation can estimate uncertainty such as ground effects. In study of [17], two types of controllers (classical PD and hybrid fuzzy PD), have been designed in order to control a quadrotor. For the simulation, MATLAB-Simulink has been used to compare the performance of these controllers in terms of attitude and position control. Moreover, some experimental tests were implemented on a manufactured test stand to control only the yaw (heading) angle. The results showed that although both methods could control the system properly, the fuzzy PD controller performed better than PD controller, especially in rejecting disturbances. An HIL simulation platform is presented in [18] to verify the image-based object tracking method adopted in small unmanned aerial vehicles. The platform consists of image processing module, scene generation module, and flight control module. To verify the performance of the HIL system, a SURF-based object tracking method is developed and tested in the case of vertical movement of the target object. An asymptotic tracking controller, using the sliding mode control and invariance based adaptive control strategy, is presented in [19]. Using sliding mode and adaptive controllers to control the attitude and position respectively, the performance of the proposed strategy is observed on an HIL simulation test-bed. The study of [20] presents a framework in which simple robots can be designed, fabricated, and tested. Using these processes, a new scripted design for quadrotors with lightweight, low cost, and rapidly manufactured systems is introduced and the result is compared with other conventional processes. Robots generated using this process took less time and cost to design and build, but possess lower tolerance and precision. Modeling, simulation, and control design of a quadrotor and the results of flight experiments conducted on a flying platform are presented in [21]. A classical PID controller is used to control law. Once the algorithm is validated using simulations and 3D visualization, it is implemented on hardware and experiments on a test-rig. The controller worked adequately for attitude stabilization during a free flight experiment. The study of [22] deals with autonomous navigation of a quadrotor by performing autonomous behavior in GPS-denied environments. Simulation and experimental tests show effective results for behaviors, such as exploration and waypoints finding. The study of [23] presents a quadrotor flight control strategy based on the coupling of fuzzy logic and sliding mode control, using a nonlinear sliding surface with the main purpose to eliminate the chattering phenomenon. Simulation results indicated that the control performance of the quadrotor was satisfactory and the proposed fuzzy sliding mode control achieved favorable tracking performance. In the mentioned study, the stability analysis was conducted for the case that the equation of the sliding surface is supposed to be crisp. However, the stability analysis for the SMC, in which the sliding surface is obtained from a fuzzy algorithm, is not performed.

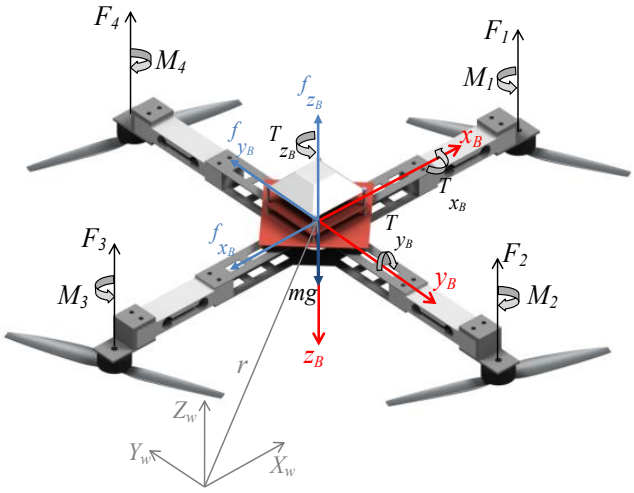

Fig. 1. Quadrotor configuration coordinate systems with global frame W and body frame B

The aim of this study is to design and control a Hardware-In-the-Loop system for quadrotor flight simulation, which enables the researcher not only to control the rotational motion, but to also simulate the translational motion of a quadrotor using exact kinetics equations alongside geometrical parameters of the physical system.

Among various control strategies which are implemented on different HIL simulators, this survey tries to benefit simultaneously from major characteristics of fuzzy logic control and sliding mode control. Experimental assessments (section 4) from the HIL set-up presented in Fig. 8 indicate that SMC gives higher agility for attitude control relative to conventional PID or FLC specifically in disturbed situations. Moreover, the accuracy of FLC is higher than SMC or conventional PID in tracking nominal angular trajectory. Hence, in order to improve the performance of a quadrotor for its autonomous flight while tracking a predesigned trajectory in presence of external disturbances, such as wind in outdoor situations, external payload or the impact of other objects to the quadrotor, a combination of two major control methods, SMC and FLC, is developed to control the translational motion of an airborne quadrotor. The stability proof of the proposed algorithm is conducted using the Lyapunov stability theorem. The algorithm was applied on the designed quadrotor motion simulator system in order to justify the performance characteristics of the control system.

The paper is arranged as follows: Section 2 describes the kinematics and kinetics of the quadrotor. In section 3, the design procedure of FLC and SMC and the associated stability analysis are propounded. The description of the designed simulator, real application of the proposed algorithm and some discussions are presented in section 4. Finally in section 5, conclusions are deduced.

2- Quadrotor Setup and Mathematical Equations of Motion

The configuration known as quadrotor has been used for a long time, and its performance has been discussed in previous studies [3-6].

In Fig. 1, the general structure of a quadrotor with appropriate coordinate systems W and B, is depicted. By introducing some assumptions and definition of the Euler angles as ψ (rotation about inertial Z axis), θ (rotation about y axis), and φ (rotation about x axis), the corresponding angular and translational equations of motion are derived.

Assumptions:

The structure is rigid and symmetrical.

The center of mass and the body-fixed frame origin are coincident.

Position equations are obtained straightforwardly by applying Newton's second law as:

$$m\ddot{r} = \begin{bmatrix} 0 \\ 0 \\ -mg \end{bmatrix} + \mathbf{R} \begin{bmatrix} -f_{x_B} \\ -f_{y_B} \\ -f_{z_B} - \sum F_i \end{bmatrix} \tag{1}$$

Where $r \triangleq [X_w\ Y_w\ Z_w]^T$, m is the quadrotor's mass, f_{x_B}, f_{y_B}, and f_{z_B} are disturbance forces, F_i, $i = 1,\ldots,4$ is motor thrust, and R is the rotation matrix shown by Eq. 2. Note that the disturbance forces and torques are generated by external agents like wind in actual flight experiments.

$$\mathbf{R}(\psi,\theta,\varphi) = \mathbf{R}_z.\mathbf{R}_y.\mathbf{R}_x.\begin{bmatrix} 1 & 0 & 0 \\ 0 & -1 & 0 \\ 0 & 0 & -1 \end{bmatrix} = \begin{bmatrix} C\psi C\theta & S\psi C\varphi - C\psi S\theta S\varphi & -S\psi S\varphi - C\psi S\theta C\varphi \\ S\psi C\theta & -C\psi C\varphi - S\psi S\theta S\varphi & C\psi S\varphi - S\psi S\theta C\varphi \\ -S\theta & -C\theta S\varphi & -C\theta C\varphi \end{bmatrix} \tag{2}$$

In Eq. 2, $C\varphi \triangleq \cos\varphi$ and $S\varphi \triangleq \sin\varphi$. The corresponding velocities and positions are obtainable by time integration of Eq. 1.

From Euler's law, angular equations of quadrotor in the body frame are as:

$$\mathbf{I}\begin{bmatrix}\dot{\omega}_x\\ \dot{\omega}_y\\ \dot{\omega}_z\end{bmatrix}=\begin{bmatrix}l(F_4-F_2)-T_{x_B}\\ l(F_1-F_3)-T_{y_B}\\ M_1-M_2+M_3-M_4-T_{z_B}\end{bmatrix}- \begin{bmatrix}\omega_x\\ \omega_y\\ \omega_z\end{bmatrix}\times\mathbf{I}\begin{bmatrix}\omega_x\\ \omega_y\\ \omega_z\end{bmatrix}-\begin{bmatrix}\omega_x\\ \omega_y\\ \omega_z\end{bmatrix}\times J_r\begin{bmatrix}0\\ 0\\ \Omega_r\end{bmatrix} \quad (3)$$

Where ω_x, ω_y, and ω_z are the angular velocities in the body frame, T_{x_B}, T_{y_B}, and T_{z_B} are disturbance torques, M_i, $i=1,\ldots,4$ is the reaction moment produced by the motors. The inertial matrix I, is diagonal according to the aforementioned assumptions, $\Omega_r=\omega_1-\omega_2+\omega_3-\omega_4$ where ω_i, $i=1,\ldots,4$ is the angular velocity of the rotors, and J_r is the moment of inertia matrix of the rotors with the sole term along z axis. In a real quadrotor setup, the non-diagonal elements of an inertial matrix, I_{xy}, I_{xz}, and I_{yz} are not equal to zero, which causes model uncertainties in dynamic equations. The last term in Eq. 3 represents the gyroscopic effect of the rotors, although it only takes into account for light-weighted quadrotors [24].

Every disturbance force that is introduced to the quadrotor, regarding location, produces a disturbance torque around the body axis. The components of disturbance force, f_{x_B}, f_{y_B}, and f_{z_B} are considered in Eq.1. The resulting disturbance torques and other external torques, T_{x_B}, T_{y_B}, and T_{z_B} are presented in Eq. 3.

Since the dynamics equations of a quadrotor have been well discussed in the previous papers, further equations are presented in the Appendix section.

3- Designing Two-Staged Trajectory Tracking Algorithm of Quadrotor Flight

An important reason behind this simulator's design is to provide the opportunity of applying various control algorithms on a quadrotor system, and comparing its behavior under these algorithms in a semi-actual condition. The core part of a quadrotor's position control is the precise attitude control of the body in order to rotate the total thrust vector to a correct direction. As a result, it is first required to have a perfect understanding of attitude control in order to control the linear motion correctly. Hence, as the first step of this study, the attitude control of the quadrotor is discussed in two major parts: quadrotor stabilizing control and attitude tracking through a desired trajectory. In this study, two types of control techniques are applied on a quadrotor simulator, including a SMC and a FLC, which the fuzzy inference is based on Mamdani max-product method. The design and implementation procedures of these algorithms are described in the forthcoming sections. After implementing these controllers on the pre-discussed simulator, some comparisons are accomplished between these two control strategies, such as: investigating the ability of the controllers to stabilize the quadrotor, their accuracy in tracking the desired trajectory, maneuverability of the quadrotor with these controllers, their ability of disturbance rejection, and their robustness against uncertainties like extra masses. Finally, regarding to the attitude control results, a new algorithm is designed and implemented for translational motion control of the quadrotor as the ultimate goal of this paper. Fig. 2 presents the position control procedure of the designed quadrotor Hardware-In-the-Loop setup.

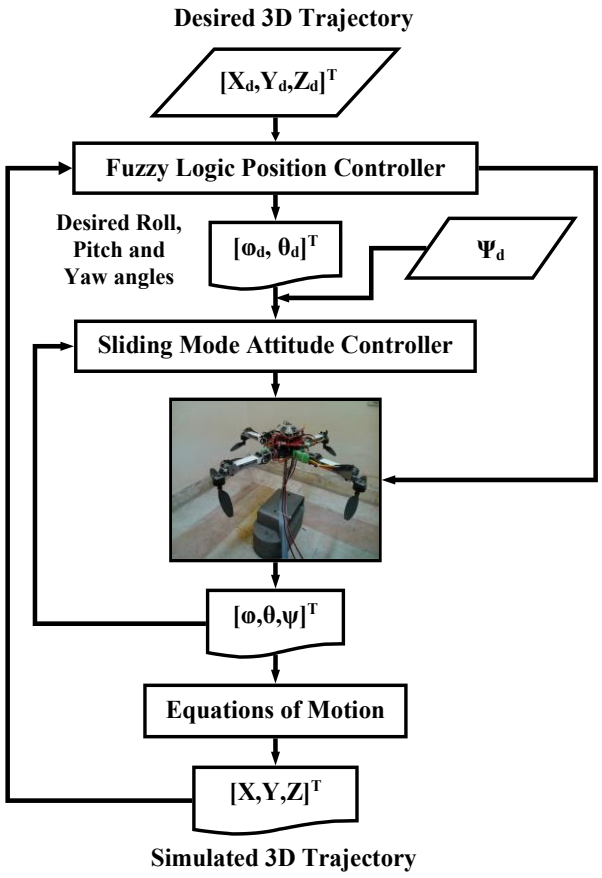

Fig. 2. Quadrotor HILMS position control procedure

3- 1- SMC-based Attitude Control

The intrinsic structure of SMC is based on the model of the system. This controller has the advantages of global stability of the system and insensitivity to parametric uncertainties and non-modeled dynamics [25-26].

According to Eq. A3, in order to design an appropriate SMC, system's dynamics is expressed as:

$$\begin{bmatrix}\ddot{\varphi}\\ \ddot{\theta}\\ \ddot{\psi}\end{bmatrix}=\begin{bmatrix}f_{\varphi}\\ f_{\theta}\\ f_{\psi}\end{bmatrix}+\begin{bmatrix}b_{11} & b_{12} & b_{13}\\ b_{21} & b_{22} & b_{23}\\ b_{31} & b_{32} & b_{33}\end{bmatrix}\begin{bmatrix}u_2\\ u_3\\ u_4\end{bmatrix} \tag{4}$$

Sliding surfaces are assumed as :

$$\begin{cases}s_{\varphi}=\dot{e}_{\varphi}+\lambda_{\varphi}e_{\varphi}\\ s_{\theta}=\dot{e}_{\theta}+\lambda_{\theta}e_{\theta}\\ s_{\psi}=\dot{e}_{\psi}+\lambda_{\psi}e_{\psi}\end{cases}, \tag{5}$$

$$\begin{cases}e_{\varphi}\triangleq\varphi_{des}(t)-\varphi(t)\\ e_{\theta}\triangleq\theta_{des}(t)-\theta(t)\\ e_{\psi}\triangleq\psi_{des}(t)-\psi(t)\end{cases},$$

$$\begin{cases}\Xi_{\varphi}\triangleq\ddot{\varphi}_{des}+\lambda_{\varphi}\dot{e}_{\varphi}\\ \Xi_{\theta}\triangleq\ddot{\theta}_{des}+\lambda_{\theta}\dot{e}_{\theta}\\ \Xi_{\psi}\triangleq\ddot{\psi}_{des}+\lambda_{\psi}\dot{e}_{\psi}\end{cases}$$

According to SMC design procedure, multiplicative gain uncertainty is presented as follows:

$$\begin{bmatrix}b_{11} & b_{12} & b_{13}\\ b_{21} & b_{22} & b_{23}\\ b_{31} & b_{32} & b_{33}\end{bmatrix}=\begin{bmatrix}1+\sigma_{11} & \sigma_{12} & \sigma_{13}\\ \sigma_{21} & 1+\sigma_{22} & \sigma_{23}\\ \sigma_{31} & \sigma_{32} & 1+\sigma_{33}\end{bmatrix}\begin{bmatrix}\hat{b}_{11} & \hat{b}_{12} & \hat{b}_{13}\\ \hat{b}_{21} & \hat{b}_{22} & \hat{b}_{23}\\ \hat{b}_{31} & \hat{b}_{32} & \hat{b}_{33}\end{bmatrix} \tag{6}$$

In which $\{\ |\sigma_{ij}|\langle Y_{ij}\ |\ i,j=1,2,3\}$, where $Y_{ij}\geq 0$. Moreover, dynamics bounds are defined as Eq. 7:

$$\begin{aligned}&\left|f_{\varphi}-\hat{f}_{\varphi}\right|\leq F_{\varphi}\\ &\left|f_{\theta}-\hat{f}_{\theta}\right|\leq F_{\theta}\\ &\left|f_{\psi}-\hat{f}_{\psi}\right|\leq F_{\psi}\end{aligned} \tag{7}$$

Using Lyapunov function, $V_i=\frac{1}{2}s_i^2$. The time derivative of this function should satisfy the following expression:

$$\dot{V}_i=\frac{1}{2}\frac{d}{dt}s_i^2\leq-\eta_i\left|s_i\right|,\qquad(\eta_i\geq 0) \tag{8}$$

Letting the control input be of the form of Eq. 9:

$$\begin{bmatrix}u_2\\ u_3\\ u_4\end{bmatrix}=\begin{bmatrix}\hat{b}_{11} & \hat{b}_{12} & \hat{b}_{13}\\ \hat{b}_{21} & \hat{b}_{22} & \hat{b}_{23}\\ \hat{b}_{31} & \hat{b}_{32} & \hat{b}_{33}\end{bmatrix}^{-1}\begin{bmatrix}-\hat{f}_{\varphi}+\Xi_{\varphi}-K_{\varphi}sgn(s_{\varphi})\\ -\hat{f}_{\theta}+\Xi_{\theta}-K_{\theta}sgn(s_{\theta})\\ -\hat{f}_{\psi}+\Xi_{\psi}-K_{\psi}sgn(s_{\psi})\end{bmatrix} \tag{9}$$

Consequently, the time derivation of the sliding surface for role angle is:

$$\begin{aligned}&\dot{s}_{\varphi}=\hat{f}_{\varphi}-f_{\varphi}+\sigma_{11}\left(-\hat{f}_{\varphi}+\Xi_{\varphi}\right)+\sigma_{12}\left(-\hat{f}_{\theta}+\Xi_{\theta}\right)+\\ &\sigma_{13}\left(-\hat{f}_{\psi}+\Xi_{\psi}\right)-\left(1+\sigma_{11}\right)K_{\varphi}sgn\left(s_{\varphi}\right)-\\ &\sigma_{12}K_{\theta}sgn\left(s_{\theta}\right)-\sigma_{13}K_{\psi}sgn\left(s_{\psi}\right)\end{aligned} \tag{10}$$

Thus, the sliding condition is verified if:

$$\begin{aligned}&\left(1-Y_{11}\right)K_{\varphi}\geq F_{\varphi}+Y_{11}\left|-\hat{f}_{\varphi}+\Xi_{\varphi}\right|+\\ &Y_{12}\left|-\hat{f}_{\theta}+\Xi_{\theta}\right|+Y_{13}\left|-\hat{f}_{\psi}+\Xi_{\psi}\right|-\\ &Y_{12}K_{\theta}-Y_{13}K_{\psi}+\eta_{\varphi}\end{aligned} \tag{11}$$

In particular, if k_{φ} is chosen:

$$\begin{aligned}&\left(1-Y_{11}\right)K_{\varphi}+Y_{12}K_{\theta}+Y_{13}K_{\psi}=\\ &F_{\varphi}+Y_{11}\left|-\hat{f}_{\varphi}+\Xi_{\varphi}\right|+Y_{12}\left|-\hat{f}_{\theta}+\Xi_{\theta}\right|+\\ &Y_{13}\left|-\hat{f}_{\psi}+\Xi_{\psi}\right|+\eta_{\varphi}\end{aligned} \tag{12}$$

The same procedures for pitch and yaw angles lead to Eq. 13:

$$\begin{aligned}&(1-\Upsilon_{22})K_{\theta}+\Upsilon_{21}K_{\varphi}+\Upsilon_{23}K_{\psi}=F_{\theta}+\\ &\Upsilon_{21}\left|-\hat{f}_{\varphi}+\Xi_{\varphi}\right|+\Upsilon_{22}\left|-\hat{f}_{\theta}+\Xi_{\theta}\right|+\Upsilon_{23}\left|-\hat{f}_{\psi}+\Xi_{\psi}\right|+\eta_{\theta}\end{aligned} \tag{13}$$

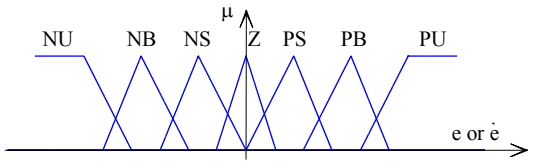

Fig. 3. Fuzzy membership functions for the input of fuzzy system in fuzzifying process

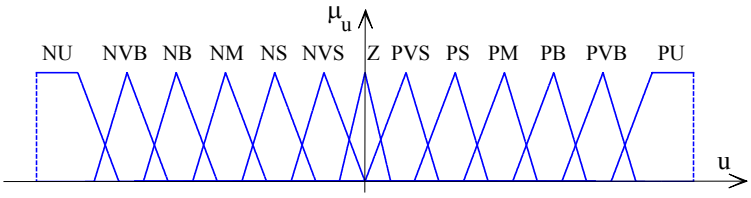

Fig. 4. Fuzzy membership functions assigned for control inputs in defuzzification process

$$(1-\Upsilon_{33})K_{\psi}+\Upsilon_{31}K_{\varphi}+\Upsilon_{32}K_{\theta}=F_{\psi}+$$

$$\Upsilon_{31}\left|-\hat{f}_{\varphi}+\Xi_{\varphi}\right|+\Upsilon_{32}\left|-\hat{f}_{\theta}+\Xi_{\theta}\right|+\Upsilon_{33}\left|-\hat{f}_{\psi}+\Xi_{\psi}\right|+\eta_{\psi}$$

Equations 12 and 13 represent a set of three equations in the three switching gains. Based on the Frobenius-Perron theorem, not only des they have unique answers for K_{φ}, K_{θ}, and K_{ψ}, but the answers are also positive (or zero) [25].

According to the Lyapunov stability theorem, the stability of equilibrium is ensured. Using the LaSalle invariance theorem, it can be ensured that by starting from a level curve of Lyapunov function, the state evolution is constrained inside the region bounded by level curve, and every point in the invariance set $s=\left\{X^s\in\Re^6:\dot{V}|_{X^s=0}\right\}$ is restricted to the equilibrium point. Using this fact, the asymptotic stability is achieved.

Since quadrotor is a nonlinear and dynamically unstable system, the parameters of SMC must be chosen carefully in order to have appropriate results. These parameters are achieved through numbers of experimental tests conducted on a real test stand. These tests indicated that if the parameters are small, the quadrotor will track the desired trajectory poorly. However, if their value is chosen to be too large, the controller's ability to reject disturbance and noise will decrease.

3- 2- FLC-based Attitude Fuzzyfier for Position Trajectory Tracking

The FLC based on Mamdani max-product method is the other approach that is chosen to control the quadrotor's attitude. The parameterized associated triangular membership functions used for this controller are shown in Fig. 3. The inputs of FLC are the errors in angles and angular velocities of the quadrotor calculated from body axis coordinate system. The main reasons for choosing triangular membership functions are simplicity of fuzzifying process and the feasibility of applying the algorithm on a real customary embedded processor.

In fuzzy systems, defuzzification process is a procedure that the linguistic variables are converted to real and numerical quantities. These numerical values will finally be applied to actuators as control inputs. Not only should this process have computational simplicity in order to be used in real-time operations, but also the small changes in variables should result small changes in control inputs [27]. Due to its cohesion and computational simplicity, the center average defuzzifier as in Eq. 14 is exerted to achieve proper control inputs:

$$y^{*}=\frac{\Sigma y_i w_i}{\Sigma w_i} \tag{14}$$

The control inputs of the system are functions of quadrotor's angles and angular velocities alongside their desired values and fuzzy logic controller parameters, as in Eq. 15. The triangular membership functions of the control inputs are demonstrated in Fig. 4. In order to have a better understanding and a precise study of Fig. 3 and 4, the quantities which are used in membership functions are shown in Fig. 5. These quantities are d_0, d_1, d_2, d_3, and d_t with different value for each variable (φ, $\dot{\varphi}$, …), which are presented in section 4.2.

$$\begin{aligned}u_2&=f_1(\varphi,\dot{\varphi},\varphi_{des},\dot{\varphi}_{des},d_0^{\varphi},d_0^{\dot{\varphi}},d_0^{u_2},r_i)\\u_3&=f_2(\theta,\dot{\theta},\theta_{des},\dot{\theta}_{des},d_0^{\theta},d_0^{\dot{\theta}},d_0^{u_3},r_i)\\u_4&=f_3(\psi,\dot{\psi},\psi_{des},\dot{\psi}_{des},d_0^{\psi},d_0^{\dot{\psi}},d_0^{u_4},r_i)\end{aligned} \tag{15}$$

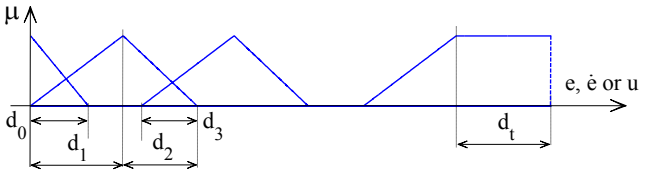

Fig. 5. Parameter clarification for fuzzy membership functions

In Fig. 5, $d_0 = r_1 d_1$, $d_2 = r_2 d_1$, $d_3 = r_3 d_1$, and $d_t = r_4 d_1$. The optimum value of r_i's and d_1 for membership functions in defuzzification steps is determined based on the experience of the designer, and are found through various kinds of trial and error searches. This step is the essential part of designing the fuzzy controller. If these parameters are chosen too large, the controller will not have the ability to reject disturbances. On the other hand, if they are chosen too small, the quadrotor will not be able to track the desired trajectory precisely. Fuzzy rules used in this controller are presented in Table 1.

With regard to Eq. A10 of the Appendix, $\mathbf{e} = \mathbf{x}_{des} - \mathbf{x}$ is the error of the system, and $\dot{\mathbf{x}}_{des} \triangleq \mathbf{g}^*(\mathbf{x}_{des}, t)$ is the time derivative of desired trajectory. It is assumed that x_{des} is a smooth and continuous function, which its time derivative can be written as a function of x_{des} and t. Due to this assumption, the function $\mathbf{g}^*(\mathbf{x}_{des}, t)$ does not contain Dirac delta function and remains bounded for all values of x_{des}.

In order to investigate the stability of the quadrotor with the proposed FLC, first the three dimensional diagram of control inputs are plotted in terms of angular error and angular velocity error. Regarding to the resulted surface, a plane's passing through the curve can be estimated as e = 0 of this surface. These surfaces for roll, pitch, and yaw angles are demonstrated in Fig. 6. Moreover, equations of the estimated surfaces are presented in Eq. 16:

$$\begin{aligned} u_2^{est} &= k_p^{\varphi} e_{\varphi} + k_d^{\varphi} \dot{e}_{\varphi} \\ u_3^{est} &= k_p^{\theta} e_{\theta} + k_d^{\theta} \dot{e}_{\theta} \\ u_4^{est} &= k_p^{\psi} e_{\psi} + k_d^{\psi} \dot{e}_{\psi} \end{aligned} \tag{16}$$

Assuming vector d as the subtraction of estimated plane and fuzzy control input in Eq. 17 and d^* as a vector of estimation error, the control input can be written as Eq. 18:

$$\mathbf{d} = \begin{bmatrix} (u_2 - u_2^{est})\,\mathrm{sgn}(e_{\varphi}) \\ (u_3 - u_3^{est})\,\mathrm{sgn}(e_{\theta}) \\ (u_4 - u_4^{est})\,\mathrm{sgn}(e_{\psi}) \end{bmatrix} \tag{17}$$

$$\mathbf{u} = \left(\boldsymbol{\kappa}_{3\times6}\mathbf{e}_{6\times1} + \mathbf{d}_{3\times1} + \mathbf{d}^*_{3\times1}\right) \tag{18}$$

Table 1. Table of fuzzy rules, (N: Negative, Z: Zero, P: Positive, VS: Very Small, S: Small, B: Big, VB: Very Big, U: Ultimate)

ė ∴ e	**NU**	**NB**	**NS**	**Z**	**PS**	**PB**	**PU**
NU	NU	NVB	NB	NM	NS	NVS	Z
NB	NVB	NB	NM	NS	NVS	Z	PVS
NS	NB	NM	NS	NVS	Z	PVS	PS
Z	NM	NS	NVS	Z	PVS	PS	PM
PS	NS	NVS	Z	PVS	PS	PM	PB
PB	NVS	Z	PVS	PS	PM	PB	PVB
PU	Z	PVS	PS	PM	PB	PVB	PU

Consequently, angular velocity's error is reformed as in Eq. 19:

$$\dot{\mathbf{e}} = \mathbf{g}^*(\mathbf{x}_{des}) - \mathbf{g}(\mathbf{x}) - \mathbf{h}_{6\times3}\left(\boldsymbol{\kappa}_{3\times6}\mathbf{e}_{6\times1} + \mathbf{d}_{3\times1} + \mathbf{d}^*_{3\times1}\right) \tag{19}$$

Where:

$$\boldsymbol{\kappa}_{3\times6} = \begin{bmatrix} k_p^{\varphi} & k_d^{\varphi} & 0 & 0 & 0 & 0 \\ 0 & 0 & k_p^{\theta} & k_d^{\theta} & 0 & 0 \\ 0 & 0 & 0 & 0 & k_p^{\psi} & k_d^{\psi} \end{bmatrix} \tag{20}$$

Lyapunov theory is used to analyze attitude stability. The Lyapunov candidate function V is presented in Eq. 21:

$$V = \frac{1}{2}\mathbf{e}^T\mathbf{P}\mathbf{e} \tag{21}$$

Where P is a 6×6 positive definite matrix. Calculating the time derivative of Eq. 21 will lead to $\dot{V}$, as in Eq. 22:

$$\dot{V} = \frac{1}{2}\Big[\mathbf{e}^T\mathbf{P}\left(\mathbf{g}^* - \mathbf{g} - \mathbf{h}\boldsymbol{\kappa}\mathbf{e} - \mathbf{h}\mathbf{d} - \mathbf{h}\mathbf{d}^*\right) + \left(\mathbf{g}^* - \mathbf{g} - \mathbf{h}\boldsymbol{\kappa}\mathbf{e} - \mathbf{h}\mathbf{d} - \mathbf{h}\mathbf{d}^*\right)^T\mathbf{P}\mathbf{e}\Big] \tag{22}$$

By defining $\mathbf{g}$ and $\mathbf{g}^*$ as:

$$\mathbf{g} = \mathbf{g}_l + \mathbf{N}\mathbf{x}, \quad \text{and } \mathbf{g}^* = \mathbf{g}_l^* + \mathbf{N}\mathbf{x}_d \tag{23}$$

Where:

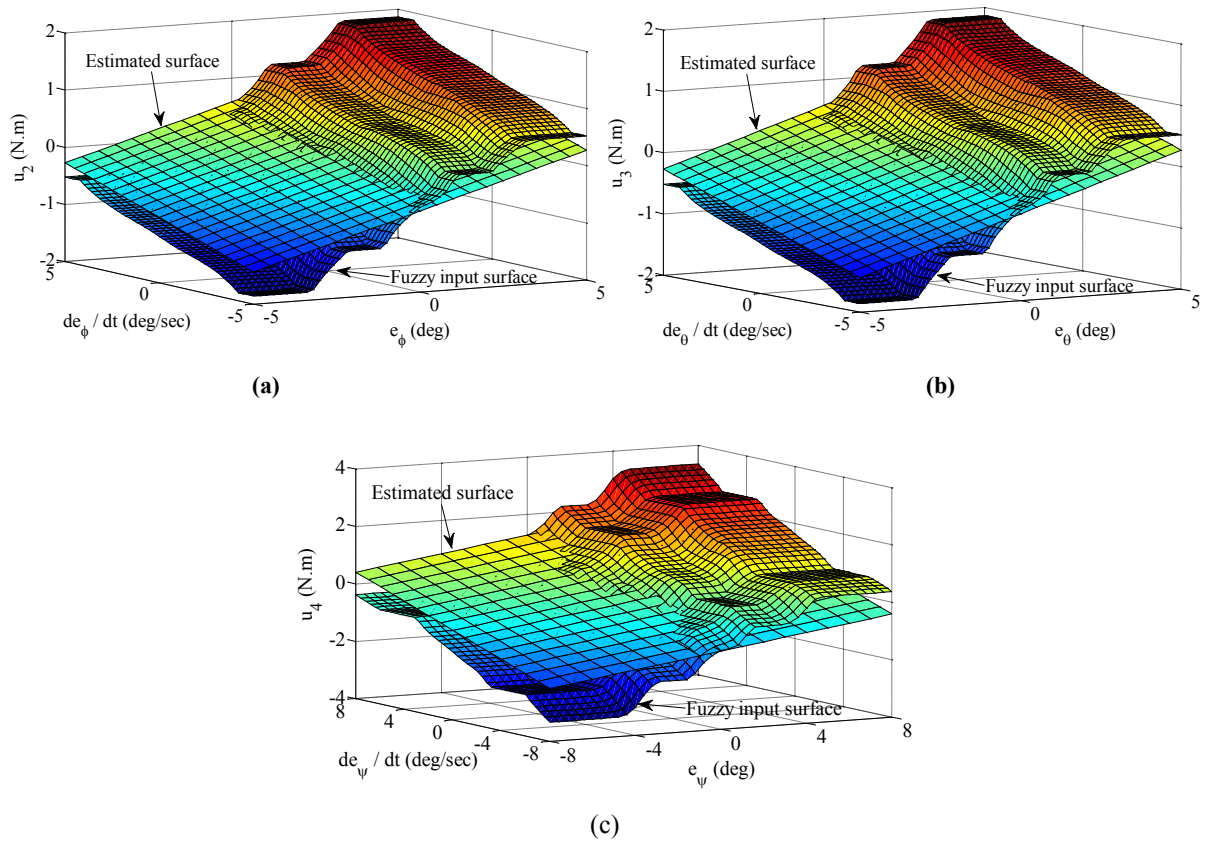

Fig. 6. FLC inputs' surfaces and their estimated planes. a) Roll angle, b) Pitch angle, c) Yaw angle

$$\mathbf{N}=\begin{bmatrix}0&1&0&0&0&0\\0&0&0&0&0&0\\0&0&0&1&0&0\\0&0&0&0&0&0\\0&0&0&0&0&1\\0&0&0&0&0&0\end{bmatrix} \tag{24}$$

Substituting Eq. 23 in Eq. 22, the time derivative of Lyapunov function, $\dot{V}$, will be achieved by Eq. 25:

$$\dot{V}=\frac{1}{2}\begin{bmatrix}-\mathbf{e}^{T}\left(\mathbf{Ph\kappa}+\boldsymbol{\kappa}^{T}\mathbf{h}^{T}\mathbf{P}+\mathbf{PN}+\mathbf{N}^{T}\mathbf{P}\right)\mathbf{e}+\\ \mathbf{eP}\left(\mathbf{g}_{1}^{*}-\mathbf{g}_{1}\right)+\left(\mathbf{g}_{1}^{*}-\mathbf{g}_{1}\right)^{T}\mathbf{Pe}-\mathbf{e}^{T}\mathbf{Phd}-\\ \mathbf{d}^{T}\mathbf{h}^{T}\mathbf{Pe}-\mathbf{e}^{T}\mathbf{Phd}^{*}-\mathbf{d}^{*T}\mathbf{h}^{T}\mathbf{Pe}\end{bmatrix} \tag{25}$$

Positive matrix H and positive scalar S are introduced in Eq. 26. From equations A11, 20, and 24 and the primary assumption about Matrix P (P is positive definite). all elements of H are positive. Additionally, S is a positive scalar because according to Eq. 17, d and e have the same sign.

$$\begin{aligned}&\mathbf{H}=\left(\mathbf{Ph\kappa}+\boldsymbol{\kappa}^{T}\mathbf{h}^{T}\mathbf{P}+\mathbf{PN}+\mathbf{N}^{T}\mathbf{P}\right),\\&\mathrm{S}=\mathbf{e}^{T}\mathbf{Phd}+\mathbf{d}^{T}\mathbf{h}^{T}\mathbf{Pe}\end{aligned} \tag{26}$$

From Eq. A11, the arguments of g_1 are either zero or multiplication of angular velocities. Regarding to the bounded thrust produced by rotors and the fact that rotors angular speed cannot have an abrupt change because of their intrinsic features and their limited rate of transceiving (transmitting and receiving) information, g_1 is always lower than a maximum value. Eq. 27 presents this fact:

$$\left(\mathbf{g}_{1}^{*}-\mathbf{g}_{1}\right)\leq\mathbf{g}_{\mathrm{Max}} \tag{27}$$

Thus, according to Eqs. 25-27, the worst scenario for Eq. 25 can be obtained from linear algebra manipulations as Eq. 28 [28]:

$$\begin{aligned}\dot{V}\leq&-\sigma_{\min}(\mathbf{H})\|\mathbf{e}\|^{2}+\sigma_{\mathrm{Max}}(\mathbf{P})\|\mathbf{g}_{\mathrm{Max}}\|\|\mathbf{e}\|-\\&\mathrm{S}+\sigma_{\mathrm{Max}}(\mathbf{Ph})\|\mathbf{d}^{*}\|\|\mathbf{e}\|\end{aligned} \tag{28}$$

Where σ(.) is the singular value of the input argument matrix. From Eq. 28, V_1 is considered as below:

$$V_1 = -\sigma_{\min}(\mathbf{H})\|\mathbf{e}\|^2 + \sigma_{\max}(\mathbf{P})\|\mathbf{g}_{\max}\|\|\mathbf{e}\| + \sigma_{\max}(\mathbf{Ph})\|\mathbf{d}^*\|\|\mathbf{e}\| \quad (29)$$

According to Eq. 17, d always has the same sign of e, meaning S is not negative. Therefore, in Eq. 30 the sufficient condition for $\dot{V}$ to be negative is $V_1 \le 0$.

$$\dot{V} \le V_1 - S \quad (30)$$

V_1 has two roots $R_1 = 0$ and R_2, presented in Eq. 31. With respect to P as a positive definite matrix, if $\|\mathbf{e}\| \ge R_2$, then $V_1 \le 0$, which results to $\dot{V} < 0$. According to Lyapunov stability theorem, the stability of the system is ensured. If $\|\mathbf{e}\| < R_2$, then $V_1 > 0$. According to Eq. 30, it is possible that $\dot{V} \ge 0$, which means that the system might be stable or unstable. If the system is unstable, the error will increase, which results to $\|\mathbf{e}\| \ge R_2$ and stability. Therefore, it can be concluded that there are two possibilities; first, if $\|\mathbf{e}\| \ge R_2$, the system is stable, and second, if $\|\mathbf{e}\| < R_2$, the system is either asymptotically stable or it includes a stable limit cycle.

$$R_2 = (\sigma_{\max}(\mathbf{P})\|\mathbf{g}_{\max}\| + \sigma_{\max}(\mathbf{Ph})\|\mathbf{d}^*\|)/\sigma_{\min}(\mathbf{H}) \quad (31)$$

Using Linear Matrix Inequality (LMI), a positive definite matrix P can be found where $V \ge 0$ and $\dot{V} < 0$, and satisfy the condition of Lyapunov stability theorem with the constraint of Eq. 32:

$$\begin{cases} \mathbf{P} > \mathbf{0} \\ \mathbf{Ph\kappa} + \boldsymbol{\kappa}^{\mathrm{T}}\mathbf{h}^{\mathrm{T}}\mathbf{P} + \mathbf{PN} + \mathbf{N}^{\mathrm{T}}\mathbf{P} > \mathbf{0} \end{cases} \quad (32)$$

The described procedure is a new method to analyze the stability of a class of fuzzy system established based on Mamdani technique. In addition, this method can be generalized to any control technique where the control input can be factorized to a linear surface and a unidirectional summing uncertainty function. With the Lyapunov stability theorem, two stability zones are achieved; first is a stable limit cycle and the other is a stable zone. Regarding to accuracy of the estimated surface, the limit cycle can be extended or shrunk. The numerical discussions of this method will be presented in section 4. 2.

In programing the HILMS, aside from using appropriate filtering method, a reasonable bound is considered for every variable or output of the sensor that was possible to overshoot or have an illogical value. Two methods were employed in order to do so. In the first method, the two successive outputs were compared. If the subtraction was more than a certain value, the previous value was used instead of the last one. Second, if the output was more than a logical value, it was ignored. For example, each impeller can produce the maximum thrust force of 850 gr.F; hence, if the output of the load cells were more than 850 gr.F, the value was considered as a false value. This way, the divergence of the equations and the instability of the setup is avoided.

3- 3- Combination of FLC Trajectory Tracking Commanding Units and SMC-based Attitude Control

In order to control the linear motion of a quadrotor, the thrust of all four propellers must be controlled precisely and simultaneously. Translational motion control is conducted in three successive steps. In the first step, the altitude of the quadrotor is controlled and the total thrust, input u_1, is the manipulated signal. The third row of Eq. 33 is used for this purpose.

Due to lack of any direct actuator to control the position of the quadrotor, the attitude should change in order to rotate the total thrust vector to the desired direction. In the second step, two virtual inputs, u_X^* and u_Y^*, are extracted from translational motion equations to allow the quadrotor to follow the desired position (X and Y) in space. From Eq. 1 and by ignoring disturbance forces the following equations are obtained.

$$\begin{aligned} m\ddot{X}_w &= u_X^*.u_1 \\ m\ddot{Y}_w &= u_Y^*.u_1 \\ m\ddot{Z}_w &= \cos\theta\cos\varphi.u_1 \end{aligned} \quad (33)$$

Where:

$$\begin{aligned} u_X^* &= (\sin\psi\sin\varphi + \cos\psi\sin\theta\cos\varphi) \\ u_Y^* &= (-\cos\psi\sin\varphi + \sin\psi\sin\theta\cos\varphi) \end{aligned} \quad (34)$$

In Eq. 33, u_1 is determined from step 1 (i.e. altitude control).

In this equation, $\nu = \left[u_X^*, u_Y^*, \cos\theta\cos\varphi\right]^{\mathrm{T}}$ is a unit vector which justifies the direction of the total thrust u_1, in order to follow the desired trajectory. u_X^* and u_Y^* are trigonometric equations and their values are always between -1 and +1. Moreover, it can easily be proved that the magnitude of ν is equal to 1, i.e. $u_X^{*2} + u_Y^{*2} + \cos^2\theta\cos^2\varphi = 1$.

The last step is to control the attitude of the quadrotor, which the desired role and pitch angles are obtained by finding the solutions of the nonlinear algebraic equations

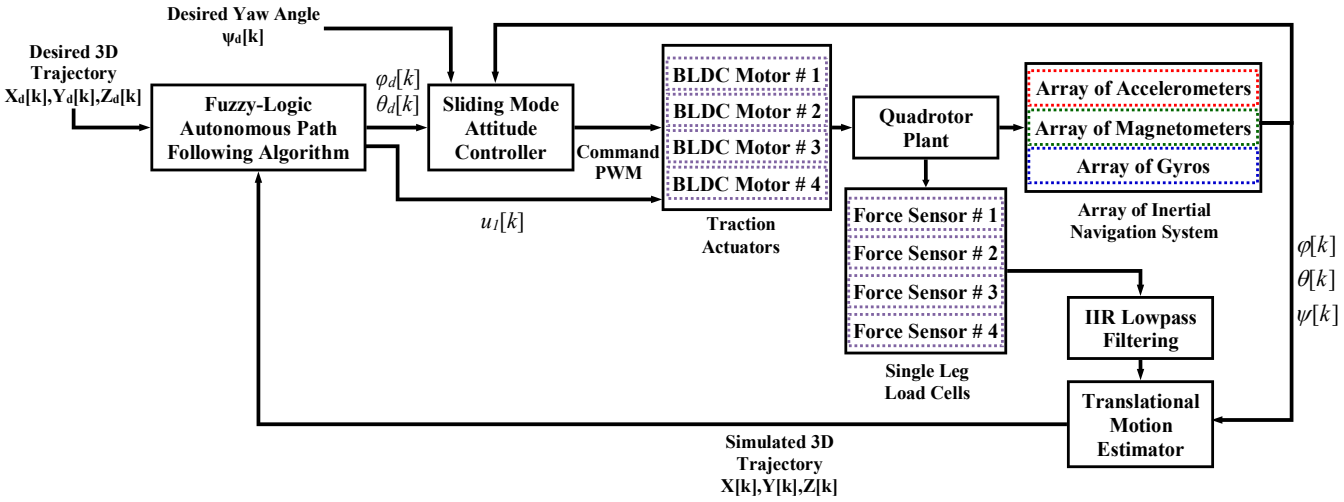

Fig. 7. Quadrotor control block diagram for proposed FLC path following SMC attitude control method

of Eq. 34. The presented solutions in Eq. 35 show that the argument of θ_d is singular when $\cos\varphi_d = 0$, $\varphi_d = k\pi \mp \frac{\pi}{2}$, and this means that quadrotor rotates 90 degrees (clockwise or counter clockwise) around its role axis. At this state, the amount of the vertical thrust along inertial Z axis is zero, hence the weight of the quadrotor cannot be compensated. In other words, maneuverability of a quadrotor is bounded, and if the angles increase significantly, total thrust vector cannot tolerate the weight of the vehicle and it will fail.

$$\varphi_d = \sin^{-1}\left(u_X.\sin\psi_d - u_Y.\cos\psi_d\right)$$
$$\theta_d = \sin^{-1}\left(\frac{u_X.\cos\psi_d + u_Y.\sin\psi_d}{\cos\varphi_d}\right) \quad (35)$$

where u_X and u_Y are obtained from fuzzy logic controller, Eq. 37.

Now that the desired angles are determined, control inputs u_2, u_3, and u_4 from Eq. A6 are used to guide the quadrotor to its desired attitude, and the process is accomplished.

In order to render the stability of the quadrotor's position control, the same approach in section 3.2 is used. The only difference is that matrix g from Eq. A10 is zero, which will only simplify the process. Additionally, in matrix h, which is presented in Eq. 36, u_1 is always positive and since role and pitch angles are limited to $-\frac{\pi}{2}$ and $\frac{\pi}{2}$, $\cos\theta\cos\varphi$ is positive as well. Consequently, by introducing a positive definite matrix P and following the same procedure, the stability proof is complete and the proposed algorithm for position control will stabilize the vehicle.

$$\mathbf{h} = \begin{bmatrix} 0 & 0 & 0 \\ u_1 & 0 & 0 \\ 0 & 0 & 0 \\ 0 & u_1 & 0 \\ 0 & 0 & 0 \\ 0 & 0 & C\theta C\varphi \end{bmatrix} \quad (36)$$

Finally, fuzzy logic position control functions of the inputs are determined as Eq. 37.

$$u_X = f_4\left(X, \dot{X}, X_{des}, \dot{X}_{des}, d_0^X, d_0^{\dot{X}}, d_0^{u_X}, r_i\right)$$
$$u_Y = f_5\left(Y, \dot{Y}, Y_{des}, \dot{Y}_{des}, d_0^Y, d_0^{\dot{Y}}, d_0^{u_Y}, r_i\right) \quad (37)$$
$$u_Z = f_6\left(Z, \dot{Z}, Z_{des}, \dot{Z}_{des}, d_0^Z, d_0^{\dot{Z}}, d_0^{u_Z}, r_i\right)$$

Fig. 7 shows the control block diagram of a quadrotor which contains two inner and outer control loops. The outer loop input is the desired translational position of the quadrotor. This desired 3D trajectory and the current position of the quadrotor are compared in fuzzy logic path following algorithm (outer loop). The resultant error in position provides input u_1 to control the altitude and the desired angular position, regarding to Eq. 35, which is the reference input of the sliding mode attitude controller (inner loop). The inner control loop uses gyros, accelerometers and the data of the magnetometers as feedback to control the attitude and to provide the inputs u_2, u_3, and u_4. The dynamics equations of the quadrotor, the applied controller to the system, and the data of the load cells are used simultaneously to calculate the required thrust of each motor in order to keep the quadrotor in

(a) (b) (c)

Fig. 8. a) Designed quadrotor simulator. b) Spherical joint used for constraining translational motion of the simulator. c) Test performance of Hardware-In-the-Loop system (https://www.youtube.com/watch?v=ZfmD3AKS3P8)

the desired position in semi-actual flight conditions. Eq. 40 in section 4.1 shows the relationship between the input voltage to the motors and the resultant thrust which is experimentally achieved using the load cells mounted on each arm of the quadrotor. Finally, using the output of the force sensors and Eq. 40, the input voltage of the motors and consequently the resulted PWM signal is computed.

4- Results and Discussions

4- 1- Quadrotor Flight Hardware-In-the-Loop Test-Bed and Calibration Procedure

This paper introduces a new approach to the design and construction of a quadrotor flight simulator using appropriate electronic circuits and mechanical elements in order to overcome the primary difficulties in rotational and translational motion control. The proposed HILMS consists of a frame connected to a spherical joint carrying the thrusting brushless DC (BLDC) motors and their electronic appendages, including the inertial navigation system. On the other hand, the BLDCs are mounted on high-precision force sensors which analogue output is read by microcontroller in real-time. These load cells are able to determine the thrust of the corresponding motor in any time during operation, which allows the simulator to estimate translational motion of a quadrotor despite of constraining it with a fully lubricated spherical joint. The embedded microcontroller makes an elaborate fusion between force sensors, gyro rates and exerts commands by a discrete-time mathematical model in order to estimate the particle position in the 3-D space. The privilege of this HILMS over other quadrotor simulators is executing experimental tests of translational motion control of the quadrotor before performing airborne tests, which prevents any potential case of instability, crashing and other relative incidents. The INS system is used to achieve the rotational position of the quadrotor, and the load cells are employed to obtain the thrust forces of the impellers. Knowing the thrust forces and the angles, the virtual position of the quadrotor can be evaluated from airborne quadrotor translational motion equations. The Hardware-In-the-Loop test-bed, which is used to simulate the quadrotor flight, is depicted in Fig. 8 (a). This setup includes a 72 MHz Cortex-M3 STM32F103RE microcontroller, an INS consisting of five 9-channel MPU6050 and magnetometer MEMS modules, four 750 KV brushless DC motors with associated 6 amperes drivers, four 26 cm puller-pusher propellers and four force sensors with 10 bit resolution and minimum readable mass of 2.44 gr.F for measuring the thrust of the motors. These load cells, commercially named ZEMIC L6D made from aluminum alloy which have a maximum capacity of 2.5 kg.F and a recommended voltage between 5 to 12 volts. These load cells are capable of measuring the thrust of each motor in an in-time mode and transfer the corresponding signal to microcontroller in order to use them in translational motion control. Consequently, combining the information of the load cells with the data from the accelerometer, gyros, and magnetometers will lead to a total thrust vector that could be justified with the help of a proper control system in order to follow a designed trajectory.

The setup is mounted on a spherical joint, shown in Fig. 8 (b), in order to allow the system to rotate without friction while avoiding translational motion. Some more associated electrical/digital/mechanical details of the test-bed are omitted. The INS system includes 5 modules, where each has a tri-axial gyroscope, accelerometer, and magnetometer. In order to obtain the angles, first the Levenberg-Marquardt algorithm is exploited to eliminate the bias error, scale factor, and axes non-orthogonality, and the data from these 5 modules were ensemble averaged to lower the adverse effects of high-frequency noises. Afterwards, an orientation estimation algorithm based on a complementary filter algorithm utilized the obtained trends where first, the dynamical accelerations decreased by a low pass filter. Since the goal of this study is not to elaborate the INS system, for further information and checking the background of inertial navigation system one can refer to author's previous papers [29-30]. The current HILMS uses the INS system along with the load cells to

Table 2. Quadrotor geometrical parameters

Parameter / Name	Current simulator	OS4 [31]	Dragan Flyer [32]
Mass (kg)	2.23	0.65	0.5
Inertia on x axis (kg.m^2)	6.2×10^{-2}	7.5×10^{-3}	4.85×10^{-3}
Inertia on y axis (kg.m^2)	6.2×10^{-2}	7.5×10^{-3}	4.85×10^{-3}
Inertia on z axis (kg.m^2)	1.16×10^{-1}	1.3×10^{-2}	8.81×10^{-3}
Arm length (m)	0.28	0.23	0.2

virtually control the translational motion of the quadrotor, studies the results of different control algorithm on the setup, and introduces an effective control method to control an airborne quadrotor in disturbed situation.

The parameters of this test-bed and two other quadrotors, provided only for a comparison purpose are listed in Table 2. These parameters which are driven from its associated CAD model are used as the geometrical parameters of the quadrotor.

A comparative study between parameters of this simulator and other quadrotors indicates that the existence of load cells and steel components increases the inertial parameters significantly. Therefore, the control system might experience larger overshoots, undershoots, and time constant. In airborne quadrotors the primary efforts are to decrease the mass of the body and inertial parameters in order to increase the battery life and load-carrying capacity. However, it is essential in Hardware-In-the-Loop systems to increase the reality of the test situation. This is the main reason of using load cells. Therefore, one has to sacrifice the former in order to achieve the later. On the other hand, this HILMS is a test-bed for testing different control algorithms and the airborne quadrotor will not use load cells and some of the steel components. In addition, when the control method is developed on the Hardware-In-the-Loop setup, it can be easily used on the airborne quadrotor by changing the controller parameters.

The relationship between thrust forces and motors reaction moment with the angular speed of the rotor can be obtained as Eq. 38 and Eq. 39, where k_F and k_M are two coefficients which could be achieved through experimental tests, and $\Omega_i, i=1,2,3,4$ is the angular velocity of the rotors.

$$F_i = k_F.\Omega_i^2 \tag{38}$$

$$M_i = k_M.\Omega_i^2 \tag{39}$$

In the current HILMS, thrust forces directly given by load cells are placed on each arm of the quadrotor. As it has been discussed, changes in thrust forces cause changes in the rotational of the quadrotor and consequently translational position. From Eq. 1, it can be observed that the position of the quadrotor is a function of role, pitch, yaw angles, and the algebraic sum of thrust forces. Therefore, the reaction moments do not directly affect the translational motion equations. Furthermore, the controlled input of attitude control, u, is obtained from SMC or FLC controllers. Consequently, it is not necessary to calculate the reaction moments of the rotors separately.

The force sensors used in this simulator create their specific noise while measuring the thrust of the motors. Due to the vibration of the arms of the simulator while the motors are in operation and the essential characteristics of the load cells, the raw output of the force sensors is not smooth and needs calibration. The raw data measured by the load cell is shown in Fig. 9 (a) which an IIR (Infinite Impulse Response) filter is used to smooth this noisy output. In order to show the reliability of load cells, a harmonic voltage is applied to brushless DC (BLDC) motors. Fig. 9(b) shows this procedure, which indicates that these load cells have the ability to follow the voltage pattern and can fairly estimate the thrusts produced by motors.

In order to calibrate the load cells, first the output bias should be removed. In Fig. 9 is shown that the output of the sensor is a number about 350 when no external force is applied. Hence, if the output of the sensor is S, the bias factor b, should be subtracted from it (S-b). In the next step, two 370 gr and 685 gr masses were applied to the arms of the simulator and the output of the corresponding load cells were observed. This way, the coefficient C is obtained to multiply into the later subtraction. The output of load cell with these masses mounted on the tail of the quadrotor is shown in Fig. 10.

By eliminating its bias and multiplying with the proper coefficient, the load cell is able to correctly evaluate the imposed force in gram force (i.e. F(gr.F)=C×(S-b)). After repeating several calibration tests and observing the load cells output while changing the input voltage, a linear relationship

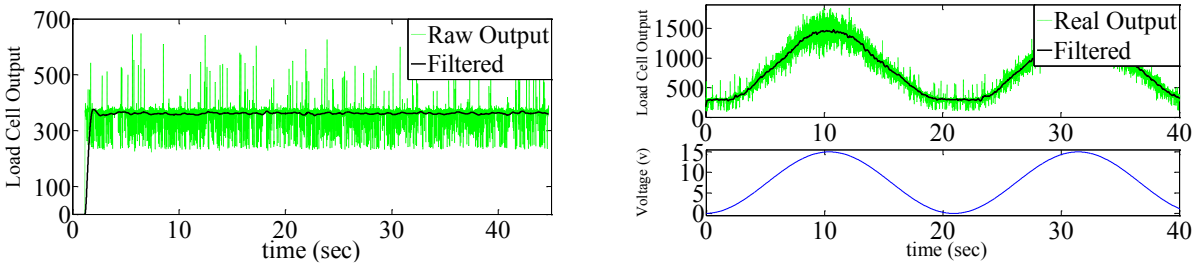

Fig. 9. Raw output of load cell (without calibration). a) Motor is not operating, b) Applied voltage to the motor follows a harmonic pattern

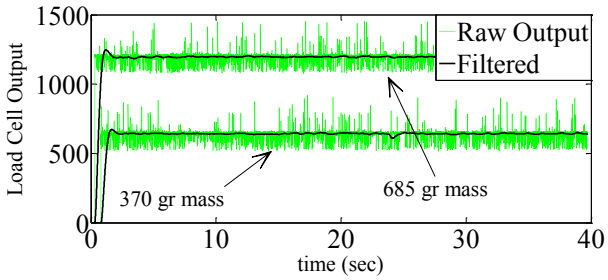

Fig. 10. Load cell's output loaded with 370gr and 685gr masses for calibration purpose

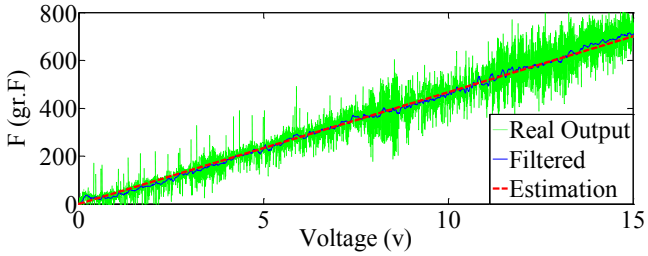

Fig. 11. The output of a load cell and its estimation while voltage changes from 0 to 15 volts

as in Eq. 40 is obtained between the applied voltage and thrust of the BLDC motor. Note that this relationship will be different depending on the type of the motor and design of the propeller.

$$F = 47.62 \times V \ (gr.F) \tag{40}$$

Calibrated and filtered output of a load cell and its estimation when the BLDC motor is in operation are shown in Fig. 11:

4- 2- Disturbance Rejection and Path Following Capabilities of the Control Algorithms

In this section, results for attitude control of the quadrotor simulator in hovering situation and tracking the desired angular trajectory are presented. For attitude control, the parameters of the sliding mode controller are presented in Eq. 41, while Table 3 represents FLC parameters, where r_1, r_2, r_3, and r_4 introduced in section 3.1.2 are equal to 0.6, 0.8, 0.6, and 1.2, respectively.

$$\begin{cases} K_\varphi = 1.47 \\ K_\theta = 1.47 \\ K_\psi = 1.42 \end{cases}, \quad \begin{cases} \lambda_\varphi = 0.17 \\ \lambda_\theta = 0.17 \\ \lambda_\psi = 0.15 \end{cases} \tag{41}$$

The numerical value of matrix $\hat{\mathbf{e}}$ for estimated surfaces in Eq. 20 is obtained as:

Table 3. The magnitude of fuzzy membership functions' parameters for attitude control

	φ	θ	ψ	$\dot{\varphi}$	$\dot{\theta}$	$\dot{\psi}$	u_2	u_3	u_4
d_1	1.8	1.8	2.5	7	7	5	0.56	0.56	0.77

$$\boldsymbol{\kappa} = \begin{bmatrix} 9.8 & 6.7 & 0 & 0 & 0 & 0 \\ 0 & 0 & 9.8 & 6.7 & 0 & 0 \\ 0 & 0 & 0 & 0 & 6.3 & 9.2 \end{bmatrix} \tag{42}$$

From these values and the geometrical parameters in Table 2, the positive definite matrix P, which is achieved from LMI, and its eigenvalues are presented in Eq. 43.

$$\mathbf{P} = \begin{bmatrix} 0.364 & 0.327 & 0 & 0 & 0 & 0 \\ 0.178 & 0.175 & 0 & 0 & 0 & 0 \\ 0 & 0 & 0.332 & 0.349 & 0 & 0 \\ 0 & 0 & 0.111 & 0.159 & 0 & 0 \\ 0 & 0 & 0 & 0 & 0.243 & 0.438 \\ 0 & 0 & 0 & 0 & 0.278 & 0.527 \end{bmatrix}, \quad \begin{cases} \lambda_1 = 0.008 \\ \lambda_2 = 0.010 \\ \lambda_3 = 0.031 \\ \lambda_4 = 0.460 \\ \lambda_5 = 0.529 \\ \lambda_6 = 0.763 \end{cases} \tag{43}$$

Fig. 12 presents the results of the tests carried out during stabilization or hover flight situation for both SMC and FLC.

In the experimental tests depicted in Fig. 12, in order to show the ability of the controllers in controlling the angles and stabilizing the quadrotor, some shocking disturbances are applied to the arms. The sharp peaks indicate the instants where these shocks are imposed to the system. The main advantage of SMC over FLC is its less settling time when the disturbance is applied. This means that the quadrotor is more agile to return to the desired state or hovering situation when an abrupt change takes place in the attitude. On the other hand, with the use of FLC, the chattering phenomenon is eliminated and the overshoot is decreased. Therefore, from this comparison, it can be concluded that FLC is more robust and SMC is more agile to the outdoor disturbances.

To show the reliability of the implemented control systems while tracking desired Euler angles φ and θ, a harmonic nominal trajectory with $\omega = 0.4$ rad/sec and the amplitude of 10 degrees, presented by Eq. 44, is introduced to the system. The result of this test is shown in Fig. 13.

$$\varphi_{des} = 10\sin(\omega t)\ (\text{degree}) \tag{44}$$

In the experimental tests conducting in this study, the desired value of yaw angle was always considered to be zero, except in Fig. 12 were disturbances were applied in order to present the effectiveness of the controllers.

In order to compare the maneuverability of the quadrotor with the implemented controllers, the frequency of the harmonic trajectory alters between relatively slow to high frequency. Mean Error (ME) in Eq. 45 is used to compare the performance of these controllers. Fig. 14 shows the ME when frequency of the above desired harmonic trajectory changes from 0.1 to 2 rad/sec. The mean average of the error for Fig. 14 is presented in Table 4.

$$ME = \frac{\sum|\varphi - \varphi_{des}|}{n} \tag{45}$$

According to Table 4, compared to the SMC, FLC has 14% and 25.3% improvement in tracking the desired roll and pitch angles, respectively. It can be inferred from Fig. 14 that the mean error for all frequencies is almost unchanged when FLC is used, meaning that the FLC has appropriate response whether the quadrotor has slow or fast maneuver, but without any external disturbances. On the other hand, the best response of SMC is when the quadrotor has a moderate maneuver, not too slow and not too fast.

Based on Figs. 12-14 and Table 4, performances of both FLC and SMC are suitable enough to be used for attitude control. In terms of tracking without disturbances, FLC shows a better response with smaller errors and more accuracy, while in terms of stabilization and rejecting disturbances, SMC has a faster response meaning that when impulsive disturbances are applied to the system, the agility of SMC to restore the quadrotor to its stability situation is more than FLC designed for this test-bed.

To show the robustness of the controllers against uncertainties, extra masses are added to two arms of the quadrotor in order to create uncertainties around the roll and pitch axis and inspect the response of the controllers to model uncertainties and their ability to restore the quadrotor to its desired state. The distance of these extra masses from the center of mass is 0.33m and this test was repeated for masses varying from 40gr to 100gr. The results for the 100gr masses are demonstrated in Fig. 15, which shows the extra masses cause chattering if disturbance is applied to the arms. This can be especially observed when the SMC is implemented on the set-up. On the other hand, it can be seen that FLC has smother response against model uncertainties, such as extra mass, in comparison to SMC; but again, it has slower response and in some cases even more overshoots.

In summary, the ability of the quadrotor to follow a desired

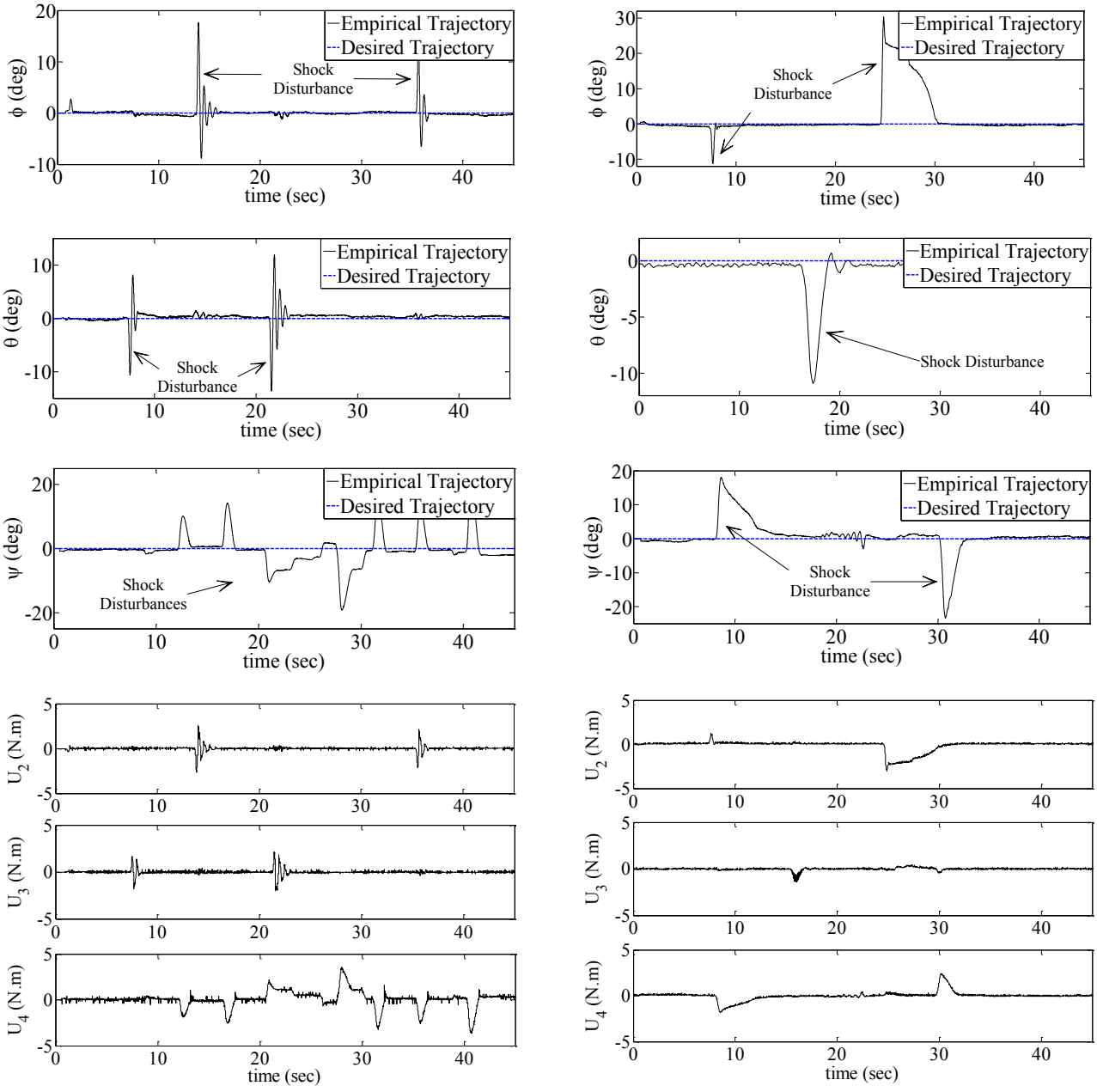

Fig. 12. Results of quadrotor stabilization control. a) SMC, b) FLC

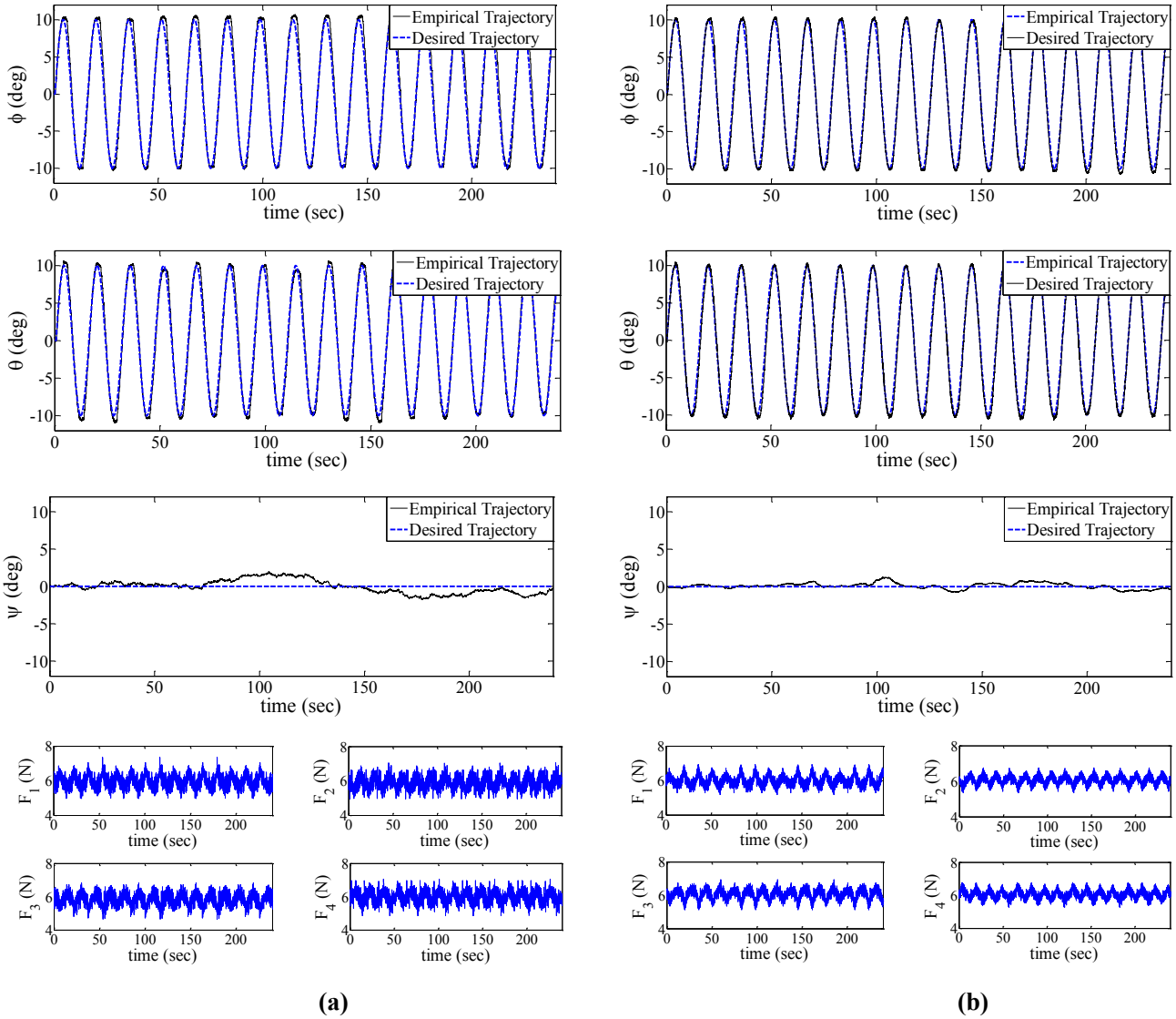

Fig. 13. Tracking the harmonic role and pitch angles with ω = 0.4 rad/sec. a) SMC, b) FLC

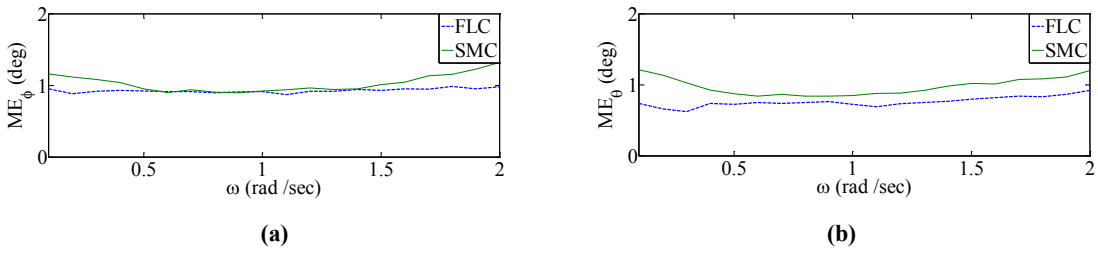

Fig. 14. Mean Error in angle versus frequency (0.1≤ω (rad/sec)≤2) when role and pitch angles follow a harmonic trajectory. a) Roll angle, b) Pitch angle

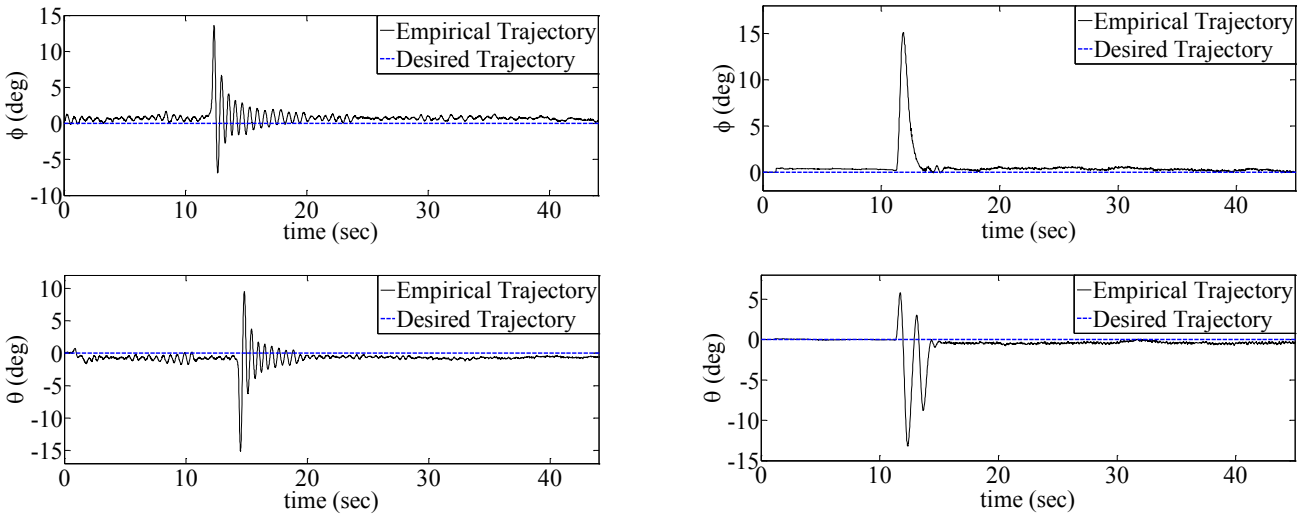

Fig. 15. Controllers' response when extra masses are added to the quadrotor' arms. a) SMC, b) FLC

Table 4. The average of ME for all different frequencies when the angles follow a harmonic pattern

Control Strategy	ME_{φ} (deg)	ME_{θ} (deg)
SMC	1.1483	1.1025
FLC	0.9854	0.8231

trajectory and its robustness against model uncertainties like extra masses with FLC is more than SMC. On the other hand, when a shock is applied in a fracture of a second and make the quadrotor off the track, the setup is more agile to restore to the original condition when using sliding mode control. The coefficients of sliding mode controller are tuned when no external mass is attached to the setup. As it is presented in Fig. 12, the results of SMC in presence of momentary disturbances are satisfying, but when a model uncertainty is applied, the performance of the controller is decreased based on Fig.15.

4- 3- Performance Evaluation of Proposed Algorithm in 3d Trajectory Tracking

The results of attitude control showed that FLC is more accurate when the situation is steady with little disturbances and the purpose of control is to follow a smooth and continuous trajectory, such as indoor filming or outdoor applications with insignificant disturbances when more precision is required. On the other hand, when a quadrotor operates in more disturbed situations, because of its agility and swift reaction toward disturbances, SMC is a better choice to control the attitude. It may cause a little chattering or vibration when disturbances are applied, but the agility of the controller compensates this negative point. Therefore, since most applications of the quadrotor are in outdoor situations with wind disturbances, SMC is a good choice to control the attitude. Moreover, since it has less control parameters, it is easier to tune a SMC. However, because of its path following ability and more precision, it is expected that FLC has better response in translational motion control.

In this paper, two strategies are used to control the translational motion of the quadrotor. First, FLC is employed to control all 6 DOFs of the quadrotor. Since quadrotor is tracking a desired trajectory in the 3D space with moderate velocity and occasional disturbances, a more effective strategy is introduced. In this strategy, a combination of SMC and FLC is used as a new method of quadrotor position control. In this method, SMC and FLC are exploited to control the angular and translational motions, respectively. Along with the trajectory tracking ability of FLC, the agility intrinsic of SMC is utilized in this method to have both precision and momentum, simultaneously.

The controller inputs for position are the error $[e_x; e_y; e_z]$ and the rate of error $[\dot{e_x}; \dot{e_y}; \dot{e_z}]$ in x, y, and z axis while the controller inputs for attitude are the error $[e_\omega; e_\theta; e_\psi]$, and the rate of error $[\dot{e_\omega}; \dot{e_\theta}; \dot{e_\psi}]$ around x, y, and z axis. The output of the controller is $[u_1; u_2; u_3; u_4; u_x; u_y]$, where u_x and u_y are the two virtual inputs that are discussed in Eq.34, and u_1, u_2, u_3, and u_4 are as A6. Additionally, both attitude and position controllers use triangular membership functions; however, the parameters are different (Table 3 and Table 5). In order to control the position of the quadrotor, the controlled inputs are selected based on the logic shown by Figs. 2 and 3, where the quantitative value of the membership function parameters is

Table 5. Fuzzy membership functions' parameters magnitude for altitude and position

	z	x	y	ż	ẋ	ẏ	u_1	u_X	u_Y
d_1	0.14	0.12	0.13	0.26	0.3	0.34	2.66	0.2	0.2

presented in Table 5.

Implementing these strategies on the simulator, and considering the desired predefined time-function trajectory first as a 3D line and then as a helix, as in Eq. 46, the results of experimental test are presented in Fig. 16.

$$X(m)=\begin{cases}0 & t<3\\ 0.3(t-3) & 3\le t<12\\ 2.5\cos\left(0.3(t-12)\right) & t\ge 12\end{cases}$$

$$Y(m)=\begin{cases}0 & t<3\\ 0.3(t-3) & 3\le t<12\\ 2.5\sin\left(0.3(t-12)\right)+2.5 & t\ge 12\end{cases} \quad (46)$$

$$Z(m)=\begin{cases}0 & t<3\\ 0.3(t-3) & 3\le t<30\\ 8 & t\ge 30\end{cases}$$

In Fig. 16, a slight delay in altitude of the quadrotor is observed. The reason is the use of IIR filter for the output of the load cells, which causes a delay in sending the thrust forces. Moreover, if the test time increases, the altitude of the quadrotor will converge to its desired value. As it is presented in Fig. 17, if the time increases to 250 seconds, the error in altitude will decrease.

The MEs for translational motion are presented in Table 6. Fig. 16 and Table 6 show the desirable performance of the controllers in the following desired trajectory. Note that with increasing the time of the test, the altitude of the quadrotor will converge to its desired value.

It can be seen from Table 6 that the proposed SMC-FLC has better response in attitude and position tracking compared to FLC. Not only does the proposed method increase the accuracy of path following, but it also develops the agility of the quadrotor to follow the evaluated angles. The results show that this controller has an improvement of about 9 % in position tracking (X and Y) compared to FLC.

Moreover, control input signals (thrust of each motor) are demonstrated in Fig. 18.

In Fig. 18, the control input signals for SMC-FLC is a thin line, while for its counterpart FLC, it is thicker. Therefore, it can be inferred that the high-frequency fluctuation of thrust forces is decreased when the SMC-FLC is implemented to control the translational motion of the quadrotor. This means that by consuming lower energy, the proposed algorithm achieves higher trajectory tracking accuracy relative to single FLC.

4- 4- Performance Evaluation of Proposed Algorithm in Way-Point Reaching, Settling and Departing

As final analysis, a discontinuous trajectory consisting of some waypoints is imposed to the simulator for position tracking. The system estimates a virtual line between the current position of the quadrotor and the next waypoint, and regarding to the remaining time in which the quadrotor should reach to its destination, it calculates the proper angle and linear velocity which is required to pass the waypoint. The algorithm used in this part greats a time-function trajectory and the quadrotor must follow that function until it reaches the vicinity of the next waypoint. When the error of the position becomes less than a definite value (here it's 8 cm), the quadrotor starts to proceed towards the next waypoint. The goal is to scrutinize the behavior of the quadrotor with the proposed control strategy when a set of waypoints are defined in the space with the same altitude and the quadrotor is supposed to move through these points. Note that it is not a regulation task since the simulator creates and tracks a virtual line between two successive points. In this test, the points are located on the vertices of a rectangular with side's length of 5 and 3 meters. The result of this inspection is depicted in Fig. 19, which shows the position of the quadrotor in a two dimensional diagram in terms of X and Y.

Fig. 19 illustrates the quadrotor's tracking performance when the position trajectory includes discontinuous terms. This figure shows that the proposed control method enables the quadrotor to move throughout the predefined waypoints with acceptable precision. In addition, mean errors for X and Y directions are 0.0923 and 0.08562 (meter), indicating the accuracy of tracking process.

The results show the superiority of the proposed SMC-FLC controller in position tracking of a quadrotor in semi-actual conditions. Since the experiments are applied on a quadrotor Hardware-In-the-Loop simulator which can appropriately simulate the translational motion of a quadrotor in outdoor situations, this control strategy can be an effective method to control a quadrotor in airborne conditions, and also a leading study for future investigations.

5- Conclusions

In this study, design and control of a simulator which can properly simulate the translational motion of a real quadrotor are discussed. The most important merits of using the proposed simulator are decreasing the casualties, which are caused by crashing and collision and minimizing the damages into nearby individuals and objects. Two control methods, including SMC and FLC based on Mamdani max-product method with triangular membership functions and center average defuzzifier, were implemented to this Hardware-In-the-Loop test-bed for attitude control of a quadrotor. Both controllers showed desirable performance when controlling the attitude. From the obtained results, it was observed that the fuzzy tracking algorithm provides better performance,

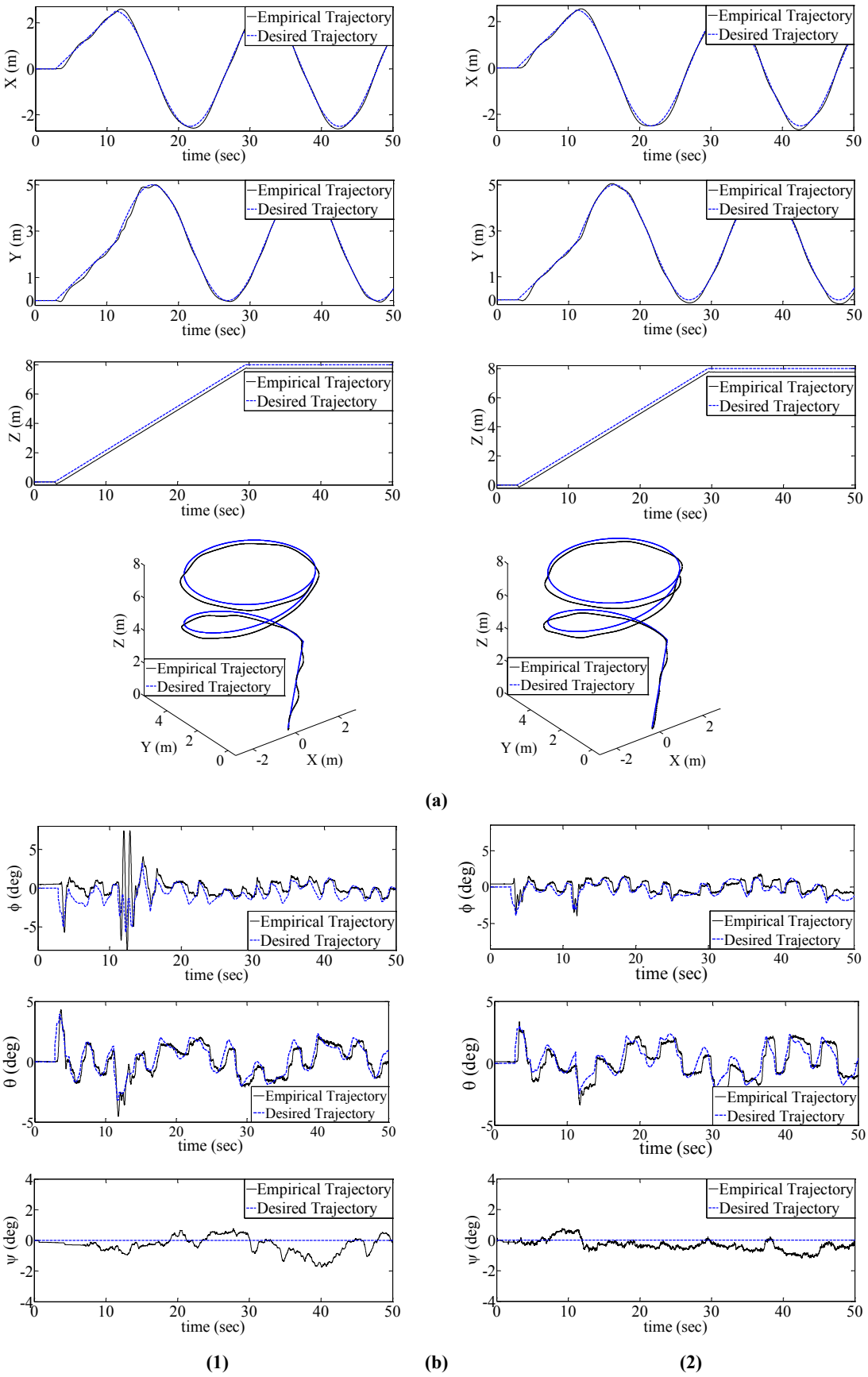

Fig. 16. a) Translational motion control of the simulator, b) Following the desired angles achieved from position tracking control. 1) FLC, 2) SMC-FLC

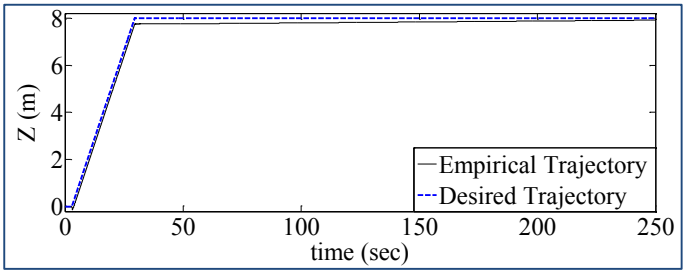

Fig. 17. Altitude of the quadrotor when the test time increases to 250 seconds

Table 6. Mean error for experimental test of position tracking

Control Strategy	ME_{φ} (deg)	ME_{θ} (deg)	ME_{ψ} (deg)	ME_{X} (m)	ME_{Y} (m)	ME_{Z} (m)
FLC	0.7460	0.5472	0.8652	0.0724	0.0607	0.2279
Combination of SMC and FLC	0.5096	0.4926	0.8197	0.0659	0.0550	0.2263

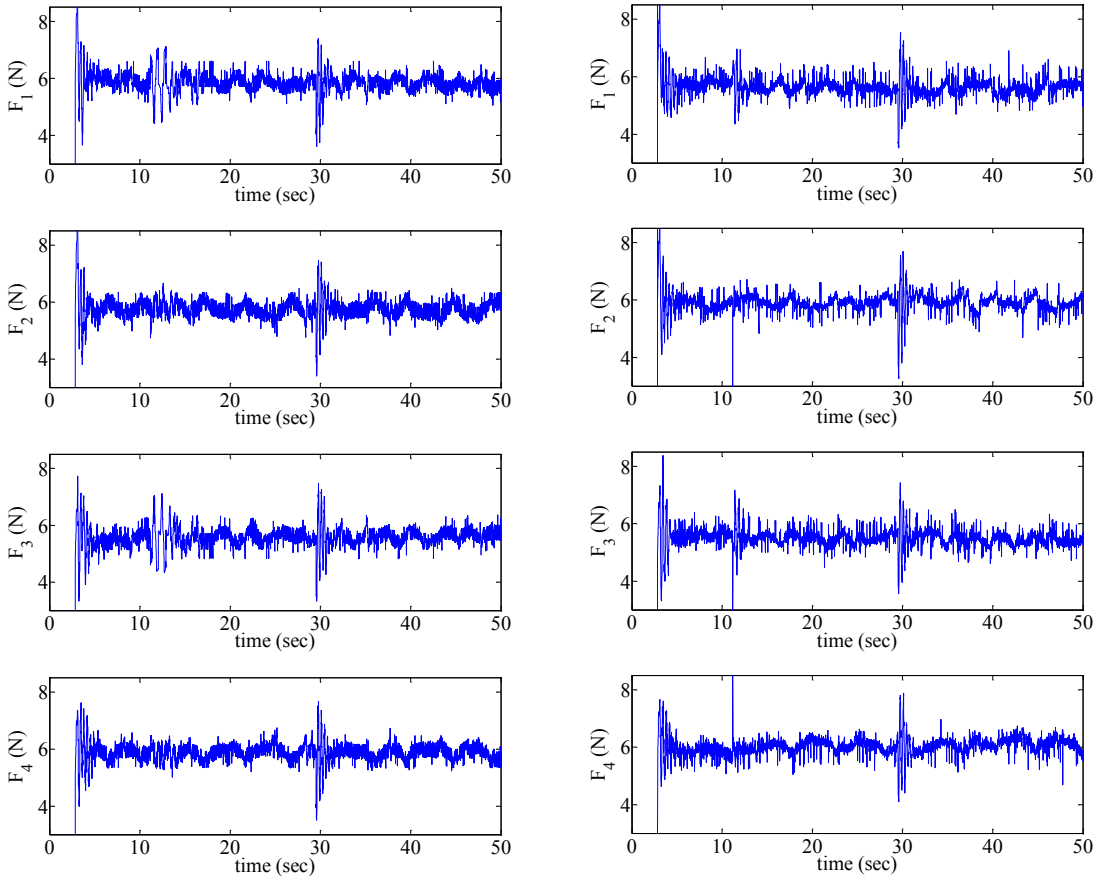

Fig. 18. Control input signals for translational motion control, a) FLC, b) SMC-FLC

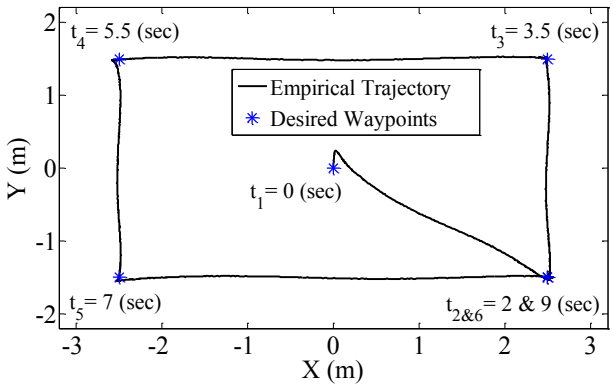

Fig. 19. Quadrotor's tracking control performance through a discontinuous trajectory

while in terms of stabilization and disturbance rejection, SMC shows faster response. Additionally, the results for robustness and uncertainty tests indicated that FLC had better results and its response in steady situations with smooth trajectories is preferable. Using the implemented force sensors and quadrotor dynamics equations of motion simultaneously, enable the simulator to estimate the translational motion. For position control of the quadrotor, first a FLC was used to control all six DOFs. Afterwards, due to the agility of SMC and path following precision of FLC, the combination of SMC and FLC was deployed to control the attitude and translational motion, respectively. The results showed that the proposed control strategy has approximately 9% accuracy improvement in tracking desired position trajectory compared to the case that only FLC is used to control all six degrees of freedom. Briefly, by combining FLC and SMC, position tracking, disturbance robustness, noise robustness, trajectory tracking accuracy, and the high frequency fluctuations of the actuators are improved simultaneously relative to the case that only FLC or SMC is used for position control of quadrotors.

List of Acronyms

FLC	Fuzzy Logic Controller
SMC	Sliding Mode Controller
HIL	Hardware-In-the-Loop
HILMS	Hardware-In-the-Loop Motion Simulator
GPS	Global Positioning System
INS	Inertial Navigation System
BFL	Backstepping Fuzzy Logic
BLMS	Backstepping Least Mean Square
CAMC	Cerebellar Model Arithmetic Computer
PID	Proportional Integral Derivative
LQR	Linear Quadratic Regulator
LMI	Linear Matrix Inequality
BLDC	Brushless Direct Current (motor)
ME	Mean Error
IRR	Infinite Impulse Response

6- Declaration of Potential Conflict of Interest

Authors of this manuscript are members of the Department of Mechanical Engineering, K. N. Toosi University of Technology, and are not employed by any non-academic government agencies. Moreover, they are not dependent upon funding or data from any political, military or sovereignty corporation or organization.

References

[1] Lugo-Cardenas, I., Salazar, S., & Lozano, R. (2016, June). The MAV3DSim Hardware in the Loop Simulation Platform for Research and Validation of UAV Controllers. In 2016 International Conference on Unmanned Aircraft Systems (ICUAS) (pp. 1335-1341). IEEE.

[2] Lange, S., & Protzel, P. (2012, March). Cost-Efficient Mono-Camera Tracking System for a Multirotor UAV Aimed for Hardware-in-the-Loop Experiments. In International Multi-Conference on Systems, Sygnals & Devices (pp. 1-6). IEEE.

[3] Lange, S., & Protzel, P. (2012, March). Cost-Efficient Mono-Camera Tracking System for a Multirotor UAV Aimed for Hardware-in-the-Loop Experiments. In International Multi-Conference on Systems, Sygnals & Devices (pp. 1-6). IEEE.

[4] Berbra, C., Simon, D., Gentil, S., & Lesecq, S. (2009). Hardware in the loop networked control and diagnosis of a quadrotor drone. IFAC Proceedings Volumes, 42(8), 971-976.

[5] Odelga, M., Stegagno, P., Bülthoff, H. H., & Ahmad, A. (2015, November). A Setup for Multi-UAV Hardware-in-the-Loop Simulations. In 2015 Workshop on Research, Education and Development of Unmanned Aerial Systems (RED-UAS) (pp. 204-210). IEEE.

[6] Bayrakceken, M. K., Ilarslan, M., Arisoy, A., & Karamancioglu, A. (2010). HILSim for attitude control of a quadrotor. In Unmanned Vehicles Workshop, UVW 2010, Proceedings of the International Workshop on Unmanned Vehicles in Istanbul/TURKEY (pp. 151-155).

[7] Nicol, C., Macnab, C. J. B., & Ramirez-Serrano, A. (2011). Robust adaptive control of a quadrotor helicopter. Mechatronics, 21(6), 927-938.

[8] Islam, S., Liu, X. P., & El Saddik, A. (2015). Adaptive sliding mode control of unmanned four rotor flying vehicle. International Journal of Robotics and Automation, 30(2).

[9] Sampath, B. G., Perera, K. C. R., Wijesuriya, W. A. S. I., & Dassanayake, V. P. C. (2014). Fuzzy Based Stabilizer Control System for Quad-Rotor. International Journal of Mechanical, Aerospace, Industrial and Mechatronics Engineering, 8(2), 455-461.

[10] Valenti, M., Bethke, B., Fiore, G., How, J. P., & Feron, E. (2006, August). Indoor multi-vehicle flight testbed for fault detection, isolation, and recovery. In Proceedings of the AIAA Guidance, Navigation, and Control Conference and Exhibit, Keystone, CO (Vol. 63, p. 64).

[11] Hoffmann, G. M., Huang, H., Waslander, S. L., & Tomlin, C. J. (2007, August). Quadrotor helicopter flight dynamics and control: Theory and experiment. In Proc. of the AIAA Guidance, Navigation, and Control Conference (Vol. 2).

[12] Castillo, P., Lozano, R., & Dzul, A. (2005). Stabilization of a mini rotorcraft with four rotors. IEEE Control Systems Magazine, 25(6), 45-55.

[13] Bouabdallah, S., Murrieri, P., & Siegwart, R. (2005). Towards autonomous indoor micro VTOL. Autonomous Robots, 18(2), 171-183.

[14] Regula, G., & Lantos, B. (2011). Backstepping based control design with state estimation and path tracking to an indoor quadrotor helicopter. Periodica Polytechnica Electrical Engineering, 53(3-4), 151-161.

[15] Pizetta, I. H. B., Brandao, A. S., & Sarcinelli-Filho, M. (2016). A Hardware-in-the-Loop Platform for Rotary-Wing Unmanned Aerial Vehicles. Journal of Intelligent & Robotic Systems, 84(1-4), 725-743.

[16] Lee, D., Kim, H. J., & Sastry, S. (2009). Feedback linearization vs. adaptive sliding mode control for a quadrotor helicopter. International Journal of control, Automation and systems, 7(3), 419-428.

[17] Erginer, B., & Altuğ, E. (2012). Design and implementation of a hybrid fuzzy logic controller for a quadrotor VTOL vehicle. International Journal of Control, Automation and Systems, 10(1), 61-70.

[18] Cheon, S. H., Ha, S. W., & Moon, Y. H. (2016, September). Hardware-in-the-loop simulation platform for image-based object tracking method using small UAV. In 2016 IEEE/AIAA 35th Digital Avionics Systems Conference (DASC) (pp. 1-5). IEEE.

[19] Zhao, B., Xian, B., Zhang, Y., & Zhang, X. (2015). Nonlinear robust sliding mode control of a quadrotor unmanned aerial vehicle based on immersion and invariance method. International Journal of Robust and Nonlinear Control, 25(18), 3714-3731.

[20] Mehta, A. M., Rus, D., Mohta, K., Mulgaonkar, Y., Piccoli, M., & Kumar, V. (2016). A scripted printable quadrotor: Rapid design and fabrication of a folded MAV. In Robotics Research(pp. 203-219). Springer, Cham.

[21] Goel, R., Shah, S. M., Gupta, N. K., & Ananthkrishnan, N. (2009). Modeling, simulation and flight testing of an autonomous quadrotor. Proceedings of ICEAE, 2009.

[22] Saeedi, S., Nagaty, A., Thibault, C., Trentini, M., & Li, H. (2016). Perception and Navigation for an Autonomous Quadrotor in GPS-denied Environments. International Journal of Robotics and Automation, 31(6).

[23] Zeghlache, S., Saigaa, D., Kara, K., Harrag, A., & Bouguerra, A. (2012). Fuzzy sliding mode control with chattering elimination for a quadrotor helicopter in vertical flight. In Hybrid Artificial Intelligent Systems (pp. 125-136). Springer Berlin Heidelberg.

[24] Sabatino, F. (2015). Quadrotor control: modeling, nonlinearcontrol design, and simulation.

[25] Slotine, J. J. E., & Li, W. (1991). Applied nonlinear control (Vol. 199, No. 1). Englewood Cliffs, NJ: Prentice-hall.

[26] Homaeinezhad, M. R., Tahbazzadeh Moghaddam, I., Khakpour, Z., & Naseri, H. (2015). Short Time Linear Quadratic Form Technique for Estimating Fast Varying Parameters in Feedback Loops. Asian Journal of Control, 17(6), 2289-2302.

[27] Wang, L. X. (1999). A course in fuzzy systems. Prentice-Hall press, USA.

[28] Bernstein, D. S. (2009). Matrix mathematics: theory, facts, and formulas. Princeton University Press.

[29] Naseri, H., & Homaeinezhad, M. R. (2014). Improving measurement quality of a MEMS-based gyro-free inertial navigation system. Sensors and Actuators A: Physical, 207, 10-19.

[30] Ghasemi Moghadam, S., & Homaeinezhad, M. R. (2018). Attitude determination by combining arrays of MEMS accelerometers, gyros, and magnetometers via quaternion based complementary filter. International Journal of Numerical Modelling: Electronic Networks, Devices and Fields, 31(3), e2282.

[31] Bouabdallah, S. (2007). Design and control of quadrotors with application to autonomous flying (Doctoral dissertation, École Polytechnique federale de Lausanne).

[32] Voos, I. (2009, April). Nonlinear control of a quadrotor micro-UAV using feedback-linearization. In Mechatronics, 2009. ICM 2009. IEEE International Conference on (pp. 1-6). IEEE.

HOW TO CITE THIS ARTICLE

H. Khajvand, M. R. Homaeinezhad, Hardware-in-the-Loop Motion Simulator of Quadrotor: Analysis of Autonomous Trajectory Tracking, AUT J. Model. Simul., 53(2) (2021) 113-136.

DOI: 10.22060/miscj.2021.19648.5241

Appendix

In order to elaborate quadrotor dynamic equations of section 2 and 3, further discussions are provided in this section.

Expanding Eq. 3 leads to:

$$\begin{aligned} I_{xx}\dot{\omega}_x &= l(F_4 - F_2) - T_{x_B} - \omega_y\omega_z(I_{zz} - I_{yy}) - \omega_y J_{r_z}\Omega_r \\ I_{yy}\dot{\omega}_y &= l(F_1 - F_3) - T_{y_B} + \omega_x\omega_z(I_{zz} - I_{xx}) + \omega_x J_{r_z}\Omega_r \\ I_{zz}\dot{\omega}_z &= -M_1 + M_2 - M_3 + M_4 - T_{z_B} - \omega_x\omega_y(I_{yy} - I_{xx}) \end{aligned} \quad (A1)$$

The relationship between the Euler angles and angular velocities of the body frame is:

$$\begin{aligned} \dot{\varphi} &= \cos\psi\sec\theta\omega_x + \sin\psi\sec\theta\omega_y \\ \dot{\theta} &= -\sin\psi\omega_x + \cos\psi\omega_y \\ \dot{\psi} &= \cos\psi\tan\theta\omega_x + \sin\psi\tan\theta\omega_y + \omega_z \end{aligned} \quad (A2)$$

By calculating the time derivative of Eq. A2, and then substituting Eqs. A1 and A2 into it, the angular motion equations are obtained as Eq. A3, where $\mathbf{x} = [\varphi, \theta, \psi]^T$ and $\mathbf{u} = [u_2, u_3, u_4]^T$:

$$\ddot{\mathbf{x}} = \mathbf{f}(\mathbf{x}) + \mathbf{b}.\mathbf{u} \quad (A3)$$

where

$$\mathbf{f}(x) = \begin{bmatrix} \sec\theta * [-\frac{1}{I_{xx}}(\cos\psi\omega_y\omega_z I_{z-y} + \omega_y J_{r_z}\Omega_r) + \frac{1}{I_{yy}}(\sin\psi\omega_x\omega_z I_{z-x} + \omega_x J_{r_z}\Omega_r) + a\dot{\theta}\tan\theta - b\dot{\psi} \\ -\frac{1}{I_{xx}}\cos\psi T_{x_B} - \frac{1}{I_{yy}}\sin\psi T_{y_B}] \\ \frac{1}{I_{xx}}(\sin\psi\omega_y\omega_z I_{z-y} + \omega_y J_{r_z}\Omega_r) + \frac{1}{I_{yy}}(\cos\psi\omega_x\omega_z I_{z-x} + \omega_x J_{r_z}\Omega_r) - a\dot{\psi} + \frac{1}{I_{xx}}\sin\psi T_{x_B} - \frac{1}{I_{yy}}\cos\psi T_{y_B} \\ -\frac{1}{I_{xx}}\cos\psi\tan\theta\omega_y\omega_z I_{z-x} + \frac{1}{I_{yy}}\sin\psi\tan\theta\omega_x\omega_z I_{z-x} - \frac{1}{I_{zz}}\omega_x\omega_y I_{y-x} + a(1+\tan^2\theta)\dot{\theta} - b\dot{\psi}\tan\theta \\ -\frac{1}{I_{xx}}\cos\psi\tan\theta T_{x_B} - \frac{1}{I_{yy}}\sin\psi\tan\theta T_{y_B} - \frac{1}{I_{zz}}T_{z_B} \end{bmatrix}_{3\times 1} \quad (A4)$$

$$\mathbf{b}(x) = \begin{bmatrix} \frac{1}{I_{xx}}\cos\psi\sec\theta & \frac{1}{I_{yy}}\sin\psi\sec\theta & 0 \\ -\frac{1}{I_{xx}}\sin\psi & \frac{1}{I_{yy}}\cos\psi & 0 \\ \frac{1}{I_{xx}}\cos\psi\tan\theta & \frac{1}{I_{yy}}\sin\psi\tan\theta & \frac{1}{I_{zz}} \end{bmatrix}_{3\times 3} \quad (A5)$$

where $I_{z\text{-}x}=(I_{zz}-I_{xx})$, $I_{z\text{-}y}=(I_{zz}-I_{yy})$, $I_{y\text{-}x}=(I_{yy}-I_{xx})$, $a=(\cos\psi\omega_x+\sin\psi\omega_y)$, and $b=(\sin\psi\omega_x-\cos\psi\omega_y)$. Finally, the control inputs are given by Eq. A6:

$$\begin{aligned} u_1 &= F_1 + F_2 + F_3 + F_4 \\ u_2 &= l(F_4 - F_2) \\ u_3 &= l(F_1 - F_3) \\ u_4 &= M_1 - M_2 + M_3 - M_4 \end{aligned} \quad (A6)$$

A quadrotor's attitude equation while hovering can be simplified as Eq. A7:

$$\begin{aligned}\ddot{\varphi} &= \frac{I_{yy}-I_{zz}}{I_{xx}}\dot{\theta}\dot{\psi} + \frac{1}{I_{xx}}u_2\\ \ddot{\theta} &= \frac{I_{zz}-I_{xx}}{I_{yy}}\dot{\varphi}\dot{\psi} + \frac{1}{I_{yy}}u_3\\ \ddot{\psi} &= \frac{I_{xx}-I_{yy}}{I_{zz}}\dot{\varphi}\dot{\theta} + \frac{1}{I_{zz}}u_4\end{aligned} \tag{A7}$$

Assuming state variables are as Eq. A8, the state-space equations are given by Eq. A9:

$$\begin{aligned}x_1 &= \varphi\\ x_2 &= \dot{\varphi}\\ x_3 &= \theta\\ x_4 &= \dot{\theta}\\ x_5 &= \psi\\ x_6 &= \dot{\psi}\end{aligned} \tag{A8}$$

$$\begin{aligned}\dot{x}_1 &= x_2\\ \dot{x}_2 &= \frac{I_{yy}-I_{zz}}{I_{xx}}x_4x_6 + \frac{1}{I_{xx}}u_2\\ \dot{x}_3 &= x_4\\ \dot{x}_4 &= \frac{I_{zz}-I_{xx}}{I_{yy}}x_2x_6 + \frac{1}{I_{yy}}u_3\\ \dot{x}_5 &= x_6\\ \dot{x}_6 &= \frac{I_{xx}-I_{yy}}{I_{zz}}x_2x_4 + \frac{1}{I_{zz}}u_4\end{aligned} \tag{A9}$$

Eq. A9 can be written in vector form as:

$$\dot{\mathbf{x}} = \mathbf{g}(\mathbf{x}) + \mathbf{h}_{6\times3}\mathbf{u}_{3\times1} \tag{A10}$$

Where:

$$\mathbf{x} = \begin{Bmatrix}x_1\\x_2\\x_3\\x_4\\x_5\\x_6\end{Bmatrix},\ \mathbf{h} = \begin{bmatrix}0 & 0 & 0\\ \frac{1}{I_{xx}} & 0 & 0\\ 0 & 0 & 0\\ 0 & \frac{1}{I_{yy}} & 0\\ 0 & 0 & 0\\ 0 & 0 & \frac{1}{I_{zz}}\end{bmatrix},\ \mathbf{g}(\mathbf{x}) = \begin{bmatrix}x_2\\ \frac{I_{yy}-I_{zz}}{I_{xx}}x_4x_6\\ x_4\\ \frac{I_{zz}-I_{xx}}{I_{yy}}x_2x_6\\ x_6\\ \frac{I_{xx}-I_{yy}}{I_{zz}}x_2x_4\end{bmatrix},\ \mathbf{u} = \begin{bmatrix}u_2\\u_3\\u_4\end{bmatrix} \tag{A11}$$

Consequently, Eq. A3 and Eq. A10 are the exact and simplified quadrotor's attitude equation, respectively.